Master's Thesis of Science
in Food Science and Biotechnology

Biochemical analysis of the cystathionine gamma-lyase MccB from *Staphylococcus aureus* and the inhibition mechanism by natural compound EGCG

황색포도상구균 유래 시스타타이오닌 감마-라이에이즈 **MccB**에 대한 생화학적 분석과 천연물의 활성 억제 메커니즘

August 2023

Food Science and Biotechnology Major
Department of Agricultural Biotechnology
The Graduate School
Seoul National University

Kyumi Byun

석사학위논문

Biochemical analysis of the cystathionine gamma-lyase MccB from *Staphylococcus aureus* and the inhibition mechanism by natural compound EGCG

지도교수 하 남 출

이 논문을 석사학위논문으로 제출함

2023년 8월

서울대학교 대학원

농생명공학부 식품생명공학전공

변 규 미

변규미의 석사학위논문을 인준함
2023년 8월

위원장	이 도 엽	(인)
부위원장	하 남 출	(인)
위원	이 기 원	(인)

Abstract

Staphylococcus aureus is a Gram-positive bacterium known for its multidrug resistance and persistent survival. Hydrogen sulfide (H_2S) has been shown to increase drug resistance and persistent survival in *S. aureus*, which mainly produces H_2S through the PLP-dependent enzyme MccB. In this study, molecular reaction mechanisms of *S. aureus* MccB was first investigated by the structural determination of the wild-type and mutant proteins. The crystal structure of the wild-type MccB protein showed some key residues near the cofactor PLP at the active site of MccB. Mutations of the residues abolished the enzymatic activities of MccB, and the crystal structures of the mutant proteins revealed that both cystathionine γ-lyase and H_2S producing activities of MccB share the catalytic residues at the active site of MccB. Also, the enzymatic activity of MccB in H_2S production and the inhibitory effects of natural compounds on this enzyme were explored. MccB exhibited a strong cystathionine γ-lyase activity producing cysteine from cystathionine and cysteine desulfhydrase activity producing H_2S from cysteine. By screening of natural compounds for their ability to inhibit SaMccB activities on cysteine, EGCG, the main constituent in tea catechins, was found to inhibit MccB enzyme activity in H_2S production. Notably, EGCG inhibited MccB by sequestering PLP, thus reducing the cytosolic pool of PLP by forming a hemi-

acetal compound with free pyridoxal or pyridoxal phosphate. EGCG also reduced the H_2S production in the SaMccB-overproducing bacteria and *Staphylococcus aureus*. Interestingly, EGCG could not inhibit the H_2S production in the *Lactobacillus plantarum*, which indicating that EGCG's inhibitory effect on the production of hydrogen sulfide may be specific to certain strains, notably *Staphylococcus aureus*. The results shed light on a novel pathway through which EGCG regulates bacterial H_2S production, and this finding may have potential applications in diets aimed at suppressing the antibiotic resistance of pathogens in gut using the edible compound EGCG.

Keywords: hydrogen sulfide, staphylococcus aureus, antibiotic resistance, MccB, cystathionine γ-lyase activity, cysteine desulfhydrase activity, pyridoxal phosphate, epigallocatechin gallate

Student Number: **2021-24928**

Contents

Abstract i

Contents iii

List of Figures v

List of Table vii

I. Introduction 1

II. Experimental Procedures 3

2.1. Plasmid construction 3

2.2. Purification of the wild-type and mutant SaMccB 3

2.2.1. Overexpression 3

2.2.2. Affinity chromatography 4

2.2.3. Ion-exchange chromatography 4

2.2.4. Size exclusion chromatography (SEC) and concentration 5

2.3. Crystallization of the wild-type and mutant SaMccB proteins 5

2.4. Data collection and structural determination 6

2.5. Enzyme kinetic assays 7

2.5.1. Measuring the cysteine desulfhydrase activity 7

2.5.2. Measuring the cystathionine γ-lyase activity 8

2.6. UV-vis and fluorescence 9

2.7. LC-MS analysis of PLP and EGCG or EGC 9

2.8. NMR analysis of the PLP-EGCG complex 10

III. Results 11

3.1. Overexpression and Purification of the wild-type SaMccB 11

3.2. Crystallization, structural determination and overall structure of the wild-type SaMccB 14

3.3. SaMccB produces H_2S through its cysteine desulfhydrase activity. 19

3.4. Overexpression, purification, crystallization, and structural determination of Y45F and S323A mutant SaMccB 22

3.5. The CSE and H_2S producing activities share the catalytic residues at the active site of MccB. 30

3.6. SaMccB exhibited the higher activities in the PLP-supplemented buffer unlike Fn1419, not requiring the additional PLP. 33

3.7. EGCG inhibits the H_2S producing activity of SaMccB. 36

3.8. EGCG make the complex with PLP in solution. 45

3.9. EGCG inhibits SaMccB by abstracting PLP from the enzyme active site. 56

3.10. Treatment of EGCG reduced the H_2S production in the SaMccB-overproducing bacteria 61

3.11. EGCG could reduce the H_2S production in the *S. aureus* whereas, it could not inhibit the H_2S production by the probiotics *Lactobacillus*...64

IV. Discussions 66

V. References 69

VI. 국문초록 71

List of Figures

Figure 1. Purification profile of the wild-type MccB protein 13

Figure 2. Crystals (left) and X-ray diffraction image (right) of the wild-type MccB.....15

Figure 3. Overall structure of MccB in the ribbon representations.....17

Figure 4. The structure of the active site of SaMccB 18

Figure 5. The cystathionine gamma-lyase and the H_2S producing activities of WT SaMccB 20

Figure 6. Purification profile of Y45F and S323A mutant MccB 26

Figure 7. Crystals (left) and X-ray diffraction image (right) of Y45F mutant MccB (top) and S323A mutant MccB (bottom) 27

Figure 8. Overall structures of the mutant MccB in the ribbon representations 28

Figure 9. The cystathionine γ-lyase and the H_2S producing activities of Y45F and S323A mutant SaMccB.....31

Figure 10. The structure of the active site of Y45F and S323A mutant SaMccB.....32

Figure 11. The absorption spectra of PLP-bound SaMccB and free-PLP....34

Figure 12. The H_2S producing activities of SaMccB with or without PLP..35

Figure 13. Screening for natural inhibitors of SaMccB.....38

Figure 14. EGCG inhibits both CSE and H_2S producing activities of

SaMccB.....40
Figure 15. Purification profile of Fn1419.....42
Figure 16. EGCG more strongly inhibits the H_2S producing activity of SaMccB than Fn1419.....43
Figure 17. Isothermal titration calorimetry of the EGCG to SaMccB and Fn1419 44
Figure 18. The absorption spectra of free-PLP, EGCG, and mixture of PLP and EGCG.....47
Figure 19. LC-MS analysis of PLP, EGCG, and mixture of PLP and EGCG 49
Figure 20. NMR analysis of PLP and EGCG complex 51
Figure 21. Chemical structures of EGCG and EGC.....52
Figure 22. LC-MS analysis of PLP, EGC, and mixture of PLP and EGC....54
Figure 23. The absorption spectra of SaMccB and Fn1419 with or without EGCG.....57
Figure 24. The absorption spectra of bound-PLP of SaMccB and Fn1419 with or without EGCG.....59
Figure 25. The H_2S producing activities of SaMccB expressing *E. coli*.....62
Figure 26. The H_2S producing activities of *S. aureus* and *L. plantarum*.....65

List of Table

Table 1. Data collection and refinement statistics 16

Table 2. Accurate mass measurements obtained from the UHPLC/TOF-HRMS Spectra of the PLP and EGCG reaction products identified.....50

Table 3. Accurate mass measurements obtained from the UHPLC/TOF-HRMS Spectra of the PLP and EGC reaction products identified 55

I. Introduction

Hydrogen sulfide (H_2S) is produced by gut bacteria and can contribute to the antibiotic resistance of pathogenic bacteria, such as *Staphylococcus aureus*, *Escherichia coli*, and *Salmonella enterica*, by decreasing oxidative stress or increasing stress response systems (Shatalin, Nuthanakanti et al. 2021). H_2S also alters the gut microbiome and promotes the growth of antibiotic-resistant bacteria (Shatalin, Nuthanakanti et al. 2021). However, H_2S plays important physiological roles in the human body, such as regulation of blood pressure, modulation of inflammation and oxidative stress, and protection against oxidative injury (Shatalin, Shatalina et al. 2011).

MccB is a PLP-dependent enzyme that catalyzes the conversion of cystathionine to cysteine, ammonia, and alpha-ketobutyrate in the methionine-to-cysteine metabolic pathway by the cystathionine γ-lyase (CSE) (Joshi, Gupta et al. 2019). MccB (or CSE) is also the major H_2S-generating enzyme of *S. aureus*, producing H_2S from cysteine via the cysteine desulfhydrase activity (Singh and Banerjee 2011). In the cysteine-to-methionine metabolic pathway, cystathionine beta-lyase (CBL) cleaves cystathionine at the beta-position, producing homocysteine and pyruvate. Both MccB and CBL are structurally homologous and require PLP for their enzymatic activities. While CBL can also produce H_2S from cysteine and homocysteine, CBL is less important in H_2S production than MccB in *S.*

aureus (Shatalin, Nuthanakanti et al. 2021).

PLP is an essential cofactor in various biological processes, including amino acid metabolism and neurotransmitter synthesis, and consists of a pyridoxal moiety and a phosphate group (Percudani and Peracchi 2003). The aldehyde group of the pyridoxal moiety allows for the formation of Schiff bases with the amine group from the enzyme or substrate, while the phosphate group provides the binding site for substrates.

Previous studies have shown that the production of H_2S by human cell-derived CBS was strongly inhibited by the natural compound EGCG (Zuhra, Petrosino et al. 2022), which is the major catechin in green tea. EGCG strongly inhibited CBS (IC50 0.3 μM) by a mixed mode by binding to the active site of the enzyme (Zuhra, Petrosino et al. 2022). However, the inhibitory effect of EGCG on the bacterial H_2S producing enzymes have been studied yet.

In this study, the roles of PLP and EGCG in the inhibition of MccB from *S. aureus* were investigated. The results further provide a novel mechanism for the inhibitory effects of EGCG against PLP-dependent enzymes, focusing on the new peak at 325 nm in UV-vis adsorption profile. The results provide insight into the molecular mechanisms underlying the control of H_2S production in the gut and could potentially aid in promoting human gut health.

II. Experimental Procedures

2.1. Plasmid construction

The gene *S. aureus* subsp. Mu50 MccB (SAV0460) was inserted into an expression vector, pLIC-His, using a ligation independent cloning method, as previously described (Lee, Jeong et al. 2019). The resulting construct pLIC-SaMccB, contained an additional 17 residues (MHHHHHHENLYFQGAAS), which encoded an N-terminal hexa-histidine tag and a TEV protease-cleavage site. After the cleavage by TEV protease, the protein retained four additional residues (GAAS) at the N-terminus. The recombinant plasmid, pLIC-SaMccB, was transformed into the expression host Escherichia coli BL21(DE3) (Novagen, Madison, WI, USA). To generate the mutant SaMccB construct (Y45F and S323A), the PCR-based mutagenesis protocol was employed using two single-primer reactions in parallel based on pLIC-SaMccB (Edelheit, Hanukoglu et al. 2009).

2.2. Purification of the wild-type and mutant SaMccB

2.2.1. Overexpression

For expression of the recombinant proteins, a single colony of *E. coli* C43 (DE3) and *E. coli* BL21 (DE3) was inoculated into 25 mL LB broth including

100 μg/mL ampicillin (Duchefa, Netherlands) and incubated at 37℃ for 14 h. Subsequently, the cells were cultured in 1.5 L Luria Broth medium containing 100 μg/mL ampicillin at 37℃ until an OD600 of 0.6 was measured, and the protein expression was induced with 0.5 mM isopropyl-β-D-thiogalactopyranoside (IPTG) at 30℃ for 6 h. The cells were harvested by centrifugation at 3850 g for 7 min. After harvest, cells were resuspended in lysis buffer containing 20 mM Tris-HCl (pH 8.0), 150 mM NaCl, and 2 mM 2-mercaptoethanol. The suspensions were disrupted using a continuous-type French press (Constant Systems Limited, United Kingdom) at 23 kpsi. The crude lysate was centrifugated at 19,000 g for 30 min at 4℃ and the pellet containing cell debris was discarded.

2.2.2. Affinity chromatography

The supernatant was loaded onto Ni^{2+}-NTA agarose resin (GE Healthcare) and rolled in a column for 45 min at 4℃. After washing the column with ~300 mL lysis buffer supplemented with 20 mM imidazole, the wild-type MccB protein was eluted with lysis buffer supplemented with 250 mM imidazole. The eluate was treated with recombinant TEV protease by incubation at room temperature for 12 h to cleave the hexahistidine tag.

2.2.3. Ion-exchange chromatography

The cleaved proteins were diluted four-fold with 20 mM Tris-HCl (pH 8.0)

buffer containing 2 mM 2-mercaptoethanol and loaded onto a HiTrap Q column (GE Healthcare, USA). A linear gradient of increasing NaCl concentration was applied to the column. The eluted fractions containing the protein were pooled and concentrated.

2.2.4. Size exclusion chromatography (SEC) and concentration

The concentrated proteins were subjected to size-exclusion chromatography using a HiLoad 26/600 Superdex 200 pg column (GE Healthcare) equilibrated with 20 mM Tris-HCl (pH 8.0) buffer containing 150 mM NaCl and 2-mercaptoethanol. The purified protein was concentrated up to 25 mg/mL using Vivaspin 20 (Sartorius, Germany) and stored at –80℃.

2.3. Crystallization of the wild-type and mutant SaMccB proteins

SaMccB proteins (wild-type, Y45F, S323A) were crystallized at 14 ℃ using the hanging drop vapor diffusion method after mixing 1 µL protein solution and 1 µL precipitation solution. The wild-type SaMccB protein was first crystallized in a precipitation solution containing 0.1M Sodium acetate (pH 4.5), 30% PEG 300. The wild-type SaMccB crystals were soaked for 20 s in a cryoprotectant buffer containing an additional 30% PEG in its own reservoir solution, and subsequently transferred into liquid nitrogen at −173 ºC to collect the dataset. Y45F mutant SaMccB was crystallized in a solution

containing 1.9 M ammonium sulfate and 0.1 M TRIS hydrochloride (pH 7.0), and S323A was crystallized in a solution containing 0.1 M MES monohydrate (pH 7.0), 1.7 M Ammonium sulfate, and 0.01 M cobalt (II) chloride hexahydrate. Crystals for Y45F and S323A mutant SaMccB were soaked for 20 s in a cryoprotectant buffer containing an additional 25% glycerol in its own reservoir solution and then flash-cooled in liquid nitrogen at −173 ºC.

2.4. Data collection and structural determination

The X-ray diffraction datasets of the wild-type, Y45F and S323A mutant SaMccB crystals were collected on an EIGER-9M detector (DECTRIS, Baden-Daettwil, Switzerland) in a beamline 5C from the Pohang Accelerator Laboratory (Pohang, Republic of Korea). The diffraction datasets were processed by the HKL-2000 program (Otwinowski and Minor 1997). The high-resolution SaMccB was determined by the molecular replacement method in the Phenix program using the low resolution wild-type SaMccB structure (PDB code: 6KHQ) as a search model. Two mutant SaMccB structures were solved using the PLP bound MccB structure in the molecular replacement method. The structure of both mutant SaMccB was determined and refined using Coot and Phenix (Adams, Afonine et al. 2010). The statistics for data collection and model refinement are summarized in Table 1.

2.5. Enzyme kinetic assays

2.5.1. Measuring the cysteine desulfhydrase activity

Fluorimetric H_2S enzymatic activity assay was performed as described previously (Thorson, Majtan et al. 2013, Druzhyna, Szczesny et al. 2016). Assays were carried out in black 96-well plate, using the H_2S-selective fluorescent probe 7-azido-4-methylcoumarin (AzMC) and a Varioskan Lux Multimode microplate reader (Thermo Fisher Scientific, USA). Enzymatic activity assays of SaMccB (2 µM/well) and MGL(2 µM/well) were carried out in Tris HCl 50 mM pH 8.0 and NaCl 150 mM containing 100 µM AzMC. The reaction samples were plated onto Corning® 96-well black polystyrene clear bottom microplates (CLS3603 Sigma–Aldrich, St. Louis, MO, USA) and incubated with pulsed shaking at 300 rpm at 37 ℃. Each well received EGCG at increasing concentration (2 µM to 200 µM), in a total assay volume of 100 µl. After 10 min incubation at 37 °C, the reaction was triggered by addition of 200 µM cysteine (final concentration). A control experiment was performed without cysteine. AMC fluorescence was measured at an excitation wavelength of 365 nm and an emission wavelength of 450 nm every 15 sec. Data were analyzed in Excel (Microsoft Corporation, Redmond, Washington, USA) and activity was estimated from the slope in the linear interval of the fluorescence increase. All images were graphed with GraphPad Prism 8 (GraphPad Software Inc.; San Diego, California, USA).

2.5.2. Measuring the cystathionine γ-lyase activity

The canonical cystathionine γ-lyase (CSE) activity utilizing cysteine and cystathionine was measured by using purified SaMccB and Fn1419 proteins. The enzymatic activity of cystathionine γ-lyase was assessed by monitoring the generation of cysteine from cystathionine. To determine the amount of cysteine generated from cystathionine, the 5,5'-dithiobis(2-nitrobenzoic acid) (DTNB) assay was employed by using a Varioskan Lux Multimode microplate reader (Thermo Fisher Scientific, USA). CSE sulfhydrase activity assays of SaMccB (2 μM/well) were carried out in Tris HCl 50 mM pH 8.0 and NaCl 150 mM containing 100 μM DTNB. The reaction samples were plated onto Corning® 96-well black polystyrene clear bottom microplates (CLS3603 Sigma–Aldrich, St. Louis, MO, USA) and incubated at 37 ℃. Each well received EGCG at increasing concentration (2 μM to 200 μM), in a total assay volume of 100 μl. After 10 min incubation at 37 °C, the reaction was triggered by addition of 200 μM cystathionine (final concentration). Absorbance of TNB formed by the reduction of DTNB by free thiol from cysteine was measured by spectrophotometrically every 15 sec. The TNB^{2-} is quantified in a spectrophotometer by measuring the absorbance of visible light at 412 nm, using an extinction coefficient of 14,150 M^{-1} cm^{-1} for dilute buffer solutions. Data were analyzed in Excel (Microsoft Corporation, Redmond, Washington, USA) and activity was estimated from the slope in the linear interval of the fluorescence increase. All images were graphed with

GraphPad Prism 8 (GraphPad Software Inc.; San Diego, California, USA).

2.6. UV-vis and fluorescence

Absorption spectra were collected on a NanoPhotometer N60 Touch (IMPLEN GMBH, München, Germany) in a buffer containing 20 mM Tris-HCl (pH 8.0), 150 mM NaCl, and 2 mM β-mercaptoethanol. All the spectra were carried out with a protein concentration of 0.1 mg/mL by successive additions of different concentrations of EGCG, and spectra were recorded between 250 nm and 500 nm after an incubation time of 1 hr at room temperature.

2.7. LC-MS analysis of PLP and EGCG or EGC

UHPLC analysis was performed by an Ultimate 3000 RSLC UHPLC system (Thermo Fisher Scientific Inc., MA, USA) equipped with a binary solvent delivery pump, auto-sampler and column oven. The UHPLC system was also equipped with Cortects C8 column (150 × 2.1 mm i.d., 1.6 µm; Waters) for the chromatographic separation of the samples. The column temperature was set at 45 °C and the injection volume was 3 µL with a flow rate of 0.25 mL/min. The mobile phases included 10 mM ammonium acetate, 0.1% formic acid in LC/MS-grade water (Solvent A) and 0.1% formic acid in LC/MS-grade methanol (Solvent B). Gradient elution consisted of 0.0–0.1 min, 0% B; 0.1–7.0 min, 20% B; 7.0–13.0 min, 90% B; 13.0–15.0 min, 90%

B; 15.0–16.0 min, 0% B; and a 4.0 min hold time for column conditioning and re-equilibration for the next analysis. High resolution mass detection was conducted with a TripleTOF 5600+ (AB SCIEX, Concord, ON, CA) operating in a negative electrospray ionization mode. The mass scan was used full scan mode with a nebulizing gas at 50 psi, a heating gas at 50 psi, and a curtain gas at 25 psi. The desolvation temperature was 500 ℃, the ion spray voltage was 4.5 kV, the collision energy was -35±15eV. The mass range was set at 70 – 1,000 m/z for MS scans.

2.8. NMR analysis of the PLP-EGCG complex

1H nuclear magnetic resonance (NMR) spectra were recorded on Bruker AV VIII 400 spectrometer. The solvent signal was used as a reference, and the chemical shifts (δ) were converted to the TMS scale (residual HDO in D2O: δH = 4.79 ppm).

III. Results

3.1. Overexpression and Purification of the wild-type SaMccB

Previous studies have shown that MccB possesses both cystathionine gamma-lyase (CSE or CGL) and H_2S producing activities in the presence of PLP-containing buffer (Lee, Jeong et al. 2019). To investigate whether purified SaMccB from *S. aureus* (SaMccB) demonstrated both activities, the full-length SaMccB proteins (380 amino acids) of *E. coli* was overexpressed and purified through affinity chromatography, anion exchange chromatography, and size exclusion chromatography (Fig. 1A-F). Each step was monitored by SDS-PAGE.

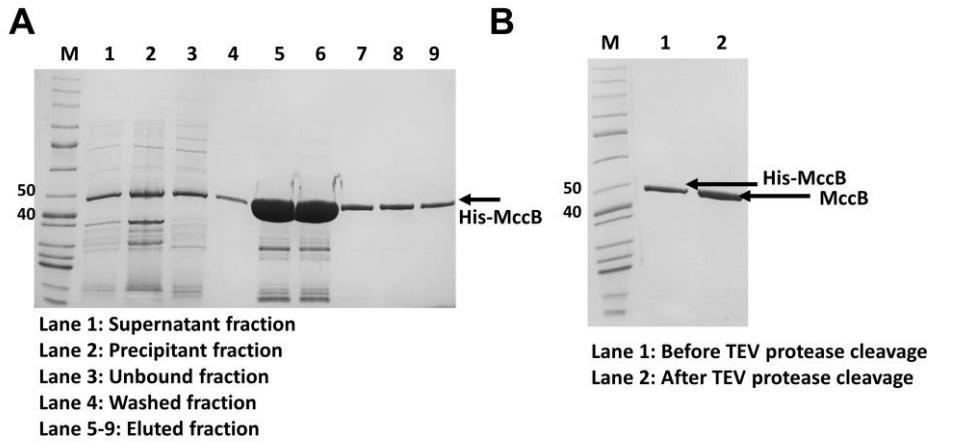

Lane 1: Supernatant fraction
Lane 2: Precipitant fraction
Lane 3: Unbound fraction
Lane 4: Washed fraction
Lane 5-9: Eluted fraction

Lane 1: Before TEV protease cleavage
Lane 2: After TEV protease cleavage

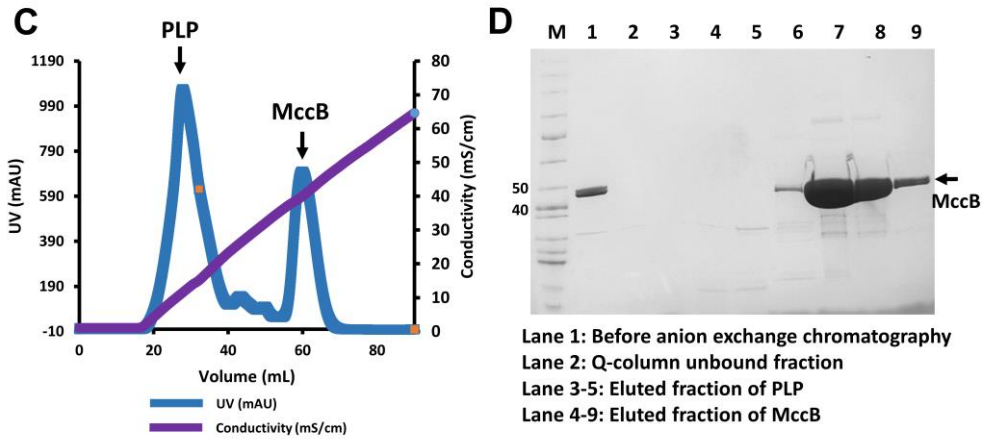

Lane 1: Before anion exchange chromatography
Lane 2: Q-column unbound fraction
Lane 3-5: Eluted fraction of PLP
Lane 4-9: Eluted fraction of MccB

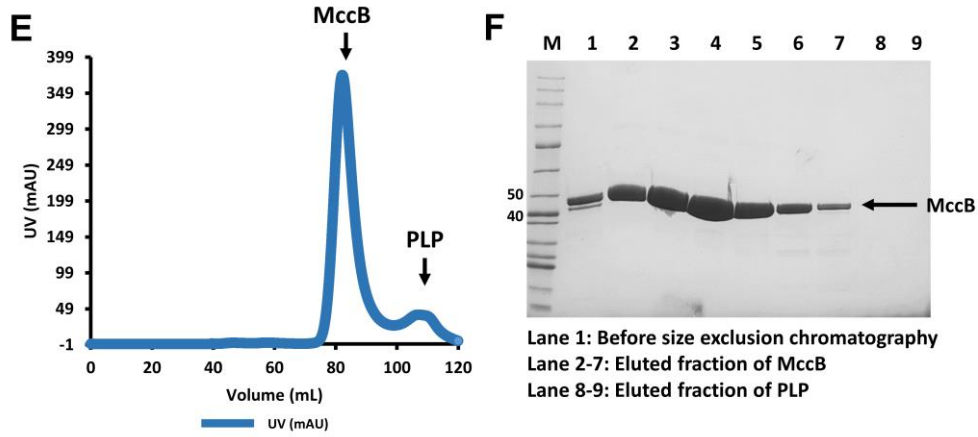

Lane 1: Before size exclusion chromatography
Lane 2-7: Eluted fraction of MccB
Lane 8-9: Eluted fraction of PLP

MccB WT

Figure 1. Purification profile of the wild-type MccB protein

A. SDS-PAGE analysis of Ni-NTA affinity chromatography

B. SDS-PAGE analysis of His-tag cleavage using TEV protease.

C. UV and conductivity diagram of the Q-column elution during the anion exchange chromatography.

D. SDS-PAGE analysis of anion exchange chromatography

E. UV diagram of the superdex column elution during the size exclusion chromatography.

F. SDS-PAGE analysis of size exclusion chromatography.

3.2. Crystallization, structural determination and overall structure of the wild-type SaMccB

It is obvious that the Lys residue (Lys196 in SaMccB) making the internal aldimine with PLP are shared with CSE and H_2S producing activities in all the PLP-dependent enzymes. However, it should be elucidated whether the CSE and H_2S producing activities shares the catalytic mechanism of SaMccB.

In this study, the crystal structure of the wild-type SaMccB was determined at a higher resolution. To gain 3D structure of SaMccB, the purified the wild-type SaMccB was concentrated up to 25 mg/mL for the crystallization. The crystals of wild-type SaMccB were obtained in the precipitant solution containing 0.1M Sodium acetate (pH 4.5) and 30% PEG 300 (Fig. 2).

The crystal structure of MccB from *S. aureus* (SaMccB) was successfully determined at 1.6 Å resolution (Fig. 2 and Table 1). The crystal of MccB belongs to the space group *I222*, with unit cell dimensions of a=62.76 Å, b=80. 1 Å, and c=161.2 Å. The asymmetric unit contained one protomer and and the tetramer was formed by the crystallographic symmetry in the crystal (Fig. 3A and 3B).

The crystal structure showed the Tyr45-containing loop and the Ser323-containing loop are lined with the substrate binding site, near the bound PLP at the active site of SaMccB (Fig. 4). Thus, the structure suggested

that Ser323 and Tyr45 are directly involved in the substrate binding.

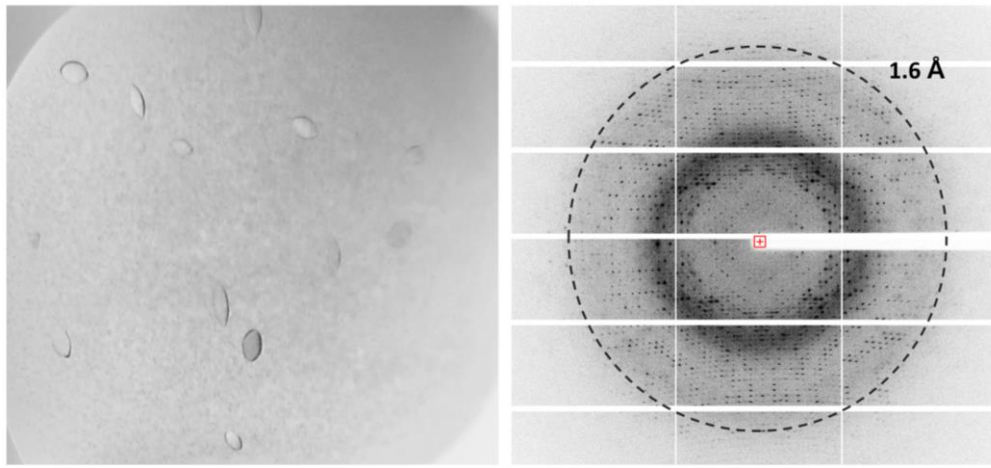

Figure 2. Crystals (left) and X-ray diffraction image (right) of the wild-type MccB

Table 1. Data collection and refinement statistics

	Wild type MccB	Y45F MccB	S323A MccB
Data collection			
Beam line	PAL 5C	PAL 5C	PAL 5C
Wavelength (Å)	1.00003	1.00003	1.00003
Space group	*I222*	*$I4_122$*	*$I4_122$*
Cell dimensions a, b, c (Å)	62.6, 80.1, 161.2	105.2, 105.2, 285.5	105.6, 105.7, 291.0
α, β, γ (°)	90, 90, 90	90, 90, 90	90, 90, 90
Resolution (Å)	50.0–1.64 (1.64–1.67)	50.0–2.20 (2.24–2.20)	50.0–2.60 (2.64–2.60)
R_{pim}	0.016 (0.086)	0.022 (0.121)	0.016 (0.114)
R_{merge}	0.0596 (0.312)	0.106 (0.603)	0.085 (0.599)
I/σ	41.6 (8.6)	31.0 (5.0)	46.75 (7.0)
Completeness (%)	97.2 (96.4)	98.8 (97.5)	100.0 (100.0)
Redundancy	13.3 (12.9)	21.1 (21.0)	26.4 (27.3)
Refinement			
Resolution (Å)	31.26–1.64	36.58–2.19	38.50–2.61
No. reflections	48,629	70298	35,329
R_{work}/R_{free}	0.2102/0.2509	0.2479/0.2376	0.2938/0.3355
No. of total atoms	3,228	2,836	2,834
Wilson B-factor (Å)	12.81	29.23	40.06
R.M.S deviations			
Bond lengths (Å)	0.01	0.009	0.004
Bond angles (°)	1.177	1.001	0.599
Ramachandran plot			
Favored (%)	98.15	97.51	97.81
Allowed (%)	1.58	2.21	1.91
Outliers (%)	0.26	0.28	0.27

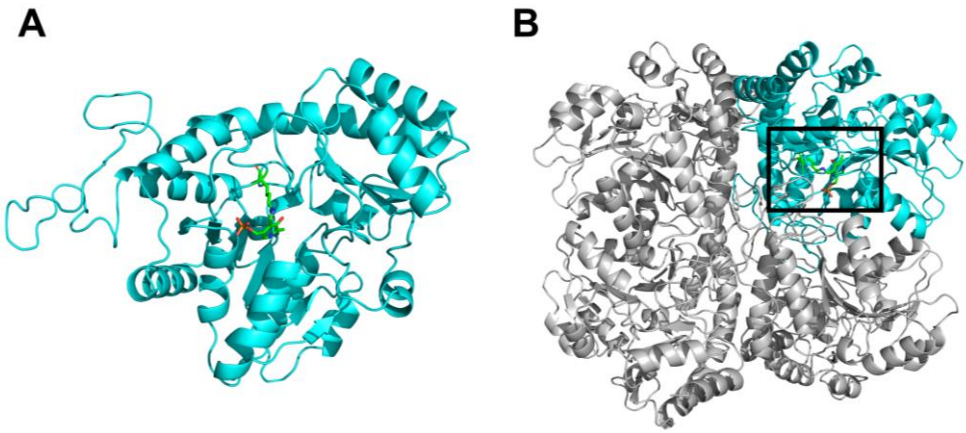

Figure 3. Overall structure of MccB in the ribbon representations

A. The asymmetric unit consists of one protomer which is depicted by the ribbon representations in cyan.

B. The tetramer structure of SaMccB. The bound PLP molecules are shown in the stick representations.

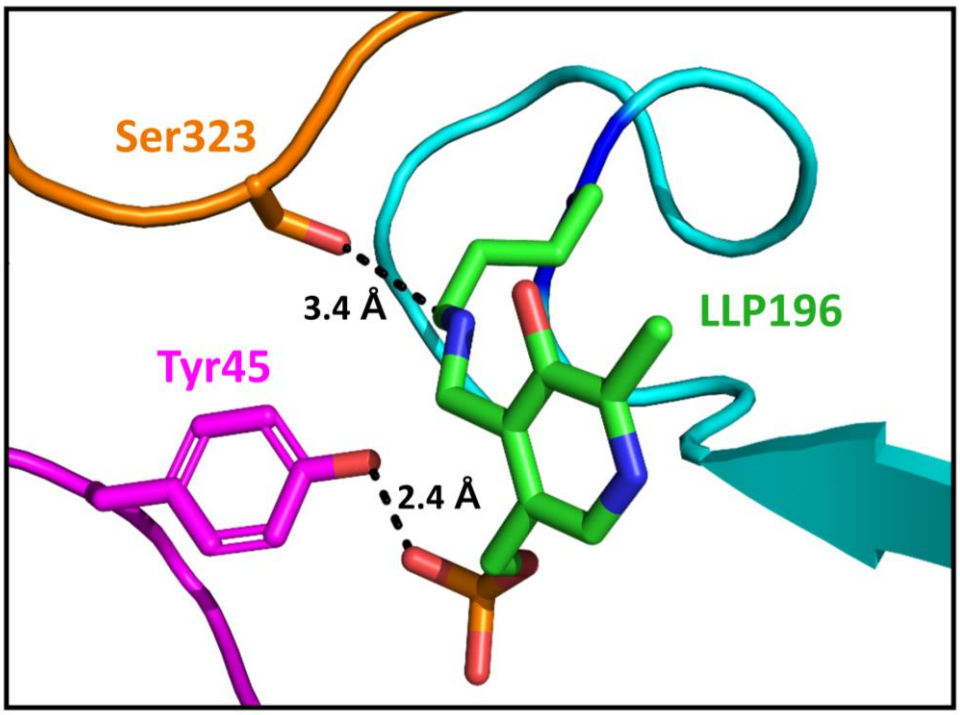

Figure 4. The structure of the active site of SaMccB

The active site of MccB. The box is enlarged from Figure 3. The bound PLP molecules are shown in the green stick representations. Each residue and PLP are labeled and indicated in the stick representations. The key interactions between the PLP (green), Tyr45 (magenta), and Ser323 (orange) are shown in black dotted lines. Distances are in Å (black).

3.3. SaMccB produces H_2S through its cysteine desulfhydrase activity.

I investigated whether purified SaMccB from *S. aureus* demonstrated both cystathionine gamma-lyase (CSE) and H_2S producing activities (Fig. 5A and 5B). The SaMccB sample was observed to break down cystathionine into compounds, including cysteine, through its CSE activity, as evidenced by the generated cysteine or free-thiol group detected by the DTNB agent.

Furthermore, the H_2S producing activity of SaMccB was assessed by measuring the amount of H_2S produced using cystathionine or cysteine as substrates (Fig. 5C). The final product, H_2S, was quantified using AzMC, as it forms a colorogenic complex with H_2S (Thorson, Majtan et al. 2013). It was likely that H_2S was generated via cysteine intermediates through the CSE activity of SaMccB, as previously observed in MccB from *E. coli* (Shatalin, Shatalina et al. 2011). Notably, the SaMccB protein exhibited higher activity in producing H_2S from cysteine than from cystathionine (Fig. 5C).

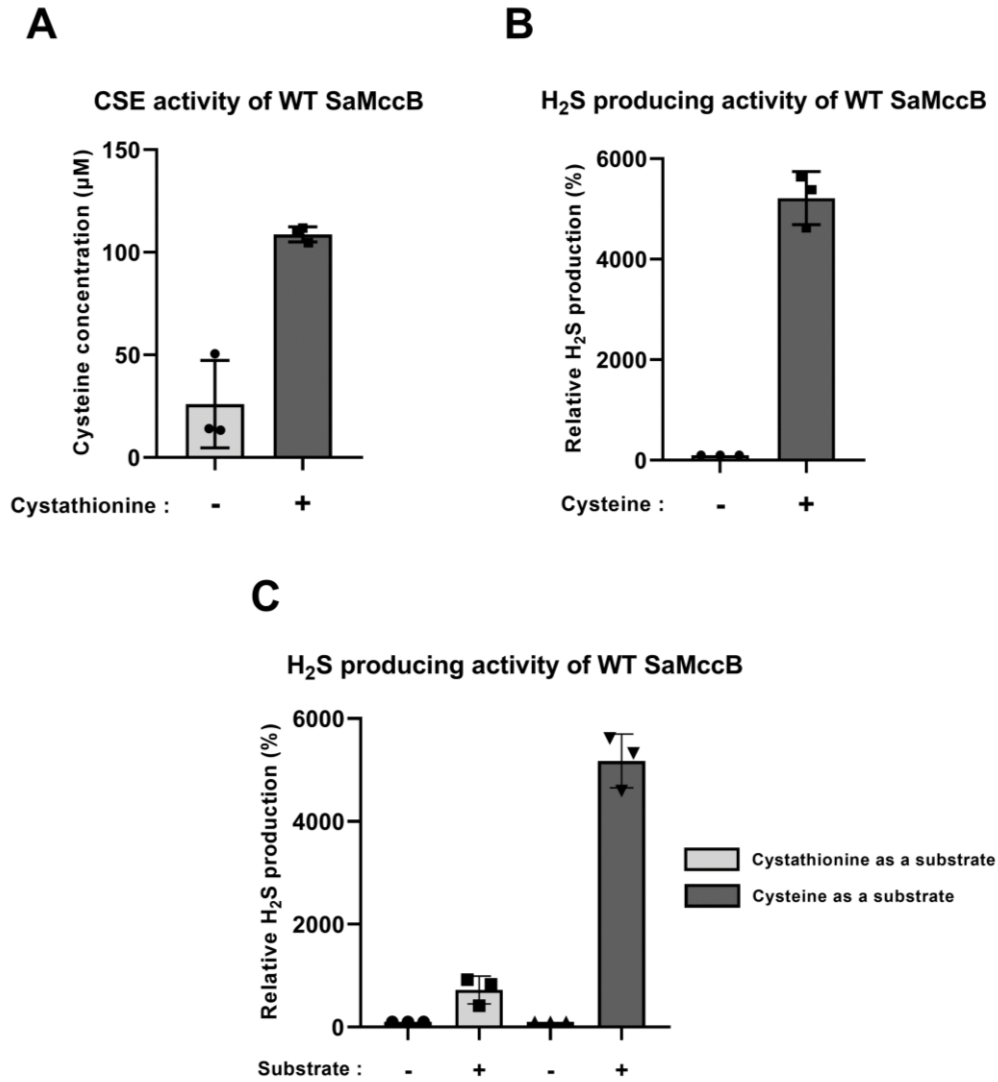

Figure 5. The cystathionine gamma-lyase and the H_2S producing activities of WT SaMccB

A. Cystathionine γ-lyase activity of WT SaMccB. The reaction was initiated by injecting 200 μM cystathionine into a buffer containing 2 μM MccB and absorbance of TNB was measured after 100 min reaction. The concentration of cysteine was determined based on the amount of the TNB generated. A control experiment was performed without

cystathionine (n = 3, mean ± SD).

B. H_2S producing activity of WT SaMccB. The reaction was initiated by injecting 200 μM cysteine into a buffer containing 2 μM MccB and fluorescence of AMC was measured after 300 min reaction. The relative H_2S production was determined based on the fluorescence of the AMC generated. A control experiment was performed without cysteine (n = 3, mean ± SD).

C. H_2S producing activity of WT SaMccB from different substrates.

3.4. Overexpression, purification, crystallization, and structural determination of Y45F and S323A mutant SaMccB

To gain the structural insights of Tyr45 and Ser323 in catalytic reaction of MccB, both mutant proteins were purified and the crystal structure of Y45F and S323A mutant SaMccB proteins were determined. Y45F and S323A mutant MccB were overexpressed and purified through affinity chromatography, anion exchange chromatography, and size exclusion chromatography. (Fig. 6A-L) Each step was monitored by SDS-PAGE.

Y45F mutant SaMccB was concentrated up to 24 mg/mL for the crystallization. The crystals of Y45F mutant SaMccB were obtained in the precipitant solution containing 2.0 M ammonium sulfate and 0.1 M TRIS hydrochloride (pH 8.5). Optimizing the precipitant solution to 1.9 M ammonium sulfate and 0.1 M TRIS hydrochloride (pH 7.0) improved the quality of Y45F mutant SaMccB crystals (Fig. 7). The crystal structure of the Y45F mutant SaMccB was determined at 2.2 Å resolution (Fig. 7 and Table 1). The crystal of MccB belongs to the space group *$I4_122$*, with unit cell dimensions of a=105.2 Å , b=105.2 Å , and c=2885.5 Å . The asymmetric unit contained one protomer and and the tetramer was formed by the crystallographic symmetry in the crystal (Fig. 8A and 8B).

S323A mutant SaMccB was concentrated up to 19 mg/mL for the crystallization. The crystals of S323A mutant SaMccB were obtained in the precipitant solution containing 0.1 M MES monohydrate (pH 6.5), 1.8 M

Ammonium sulfate, and 0.01 M cobalt (II) chloride hexahydrate. Optimizing the precipitant solution to 0.1 M MES monohydrate (pH 7.0), 1.7 M Ammonium sulfate, and 0.01 M cobalt (II) chloride hexahydrate improved the quality of S323A mutant SaMccB crystals (Fig. 7). The crystal structure of S323A mutant SaMccB was determined at 2.6 Å resolution (Fig. 7 and Table 1). The crystal of MccB belongs to the space group $I4_122$, with unit cell dimensions of a=105.6 Å, b=105.7 Å, and c=291.0 Å. The asymmetric unit contained one protomer and and the tetramer was formed by the crystallographic symmetry in the crystal (Fig. 8C and 8D).

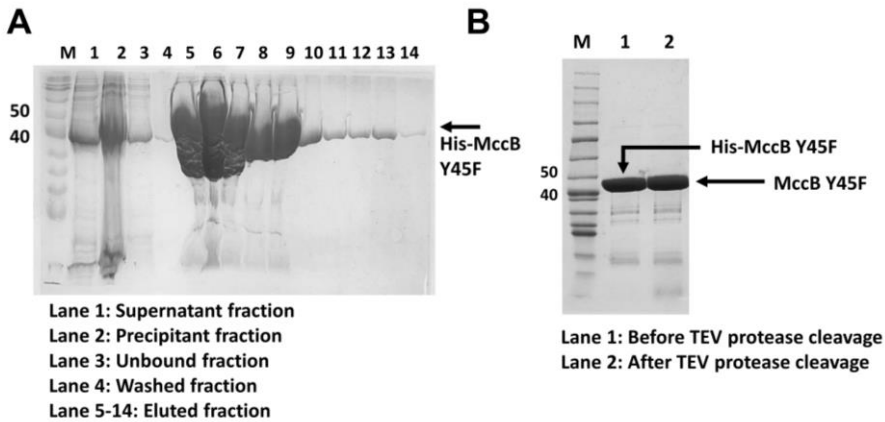

Lane 1: Supernatant fraction
Lane 2: Precipitant fraction
Lane 3: Unbound fraction
Lane 4: Washed fraction
Lane 5-14: Eluted fraction

Lane 1: Before TEV protease cleavage
Lane 2: After TEV protease cleavage

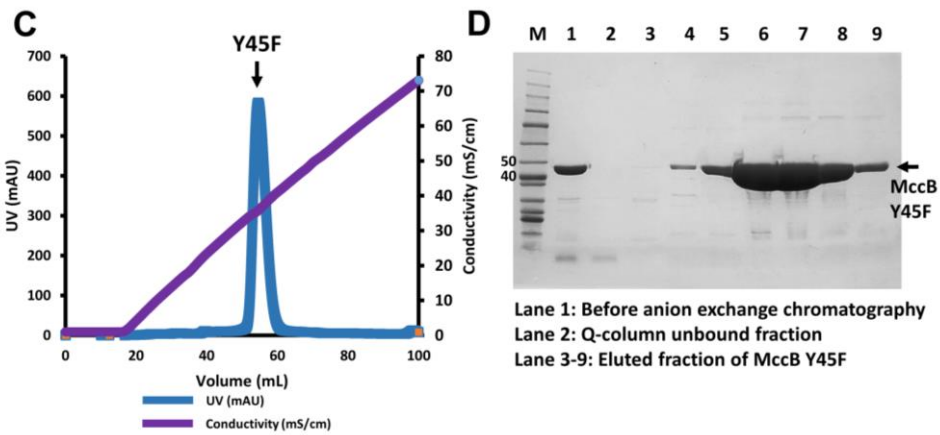

Lane 1: Before anion exchange chromatography
Lane 2: Q-column unbound fraction
Lane 3-9: Eluted fraction of MccB Y45F

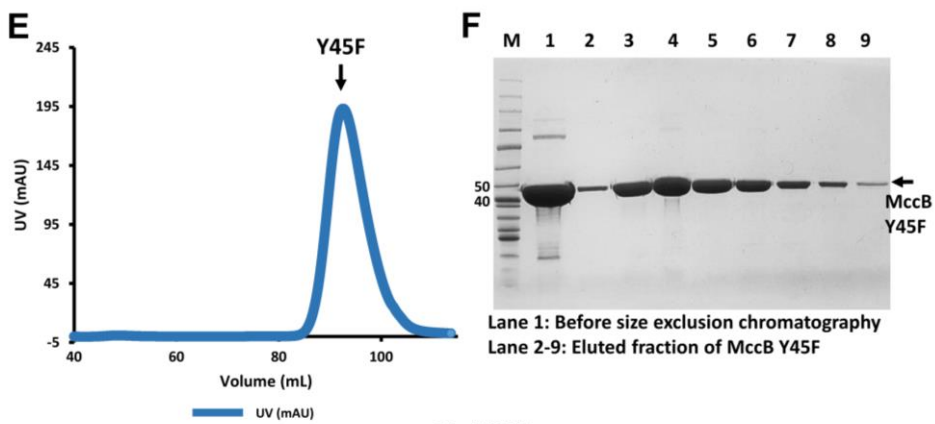

Lane 1: Before size exclusion chromatography
Lane 2-9: Eluted fraction of MccB Y45F

MccB Y45F

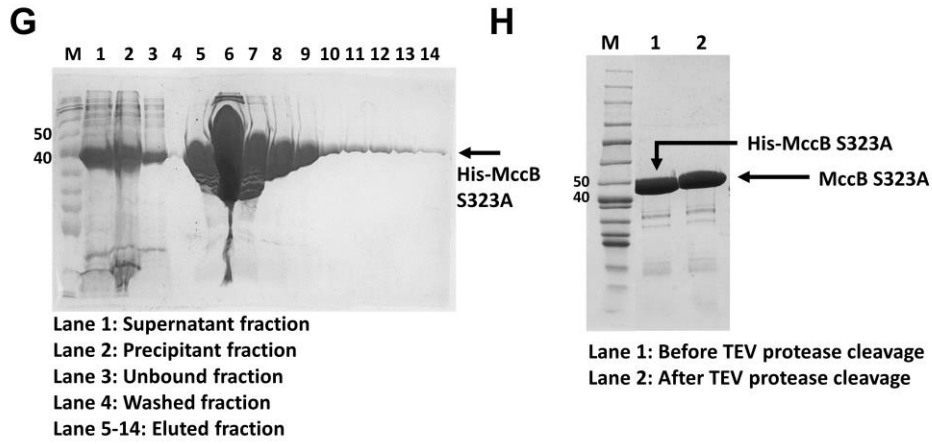

Lane 1: Supernatant fraction
Lane 2: Precipitant fraction
Lane 3: Unbound fraction
Lane 4: Washed fraction
Lane 5-14: Eluted fraction

Lane 1: Before TEV protease cleavage
Lane 2: After TEV protease cleavage

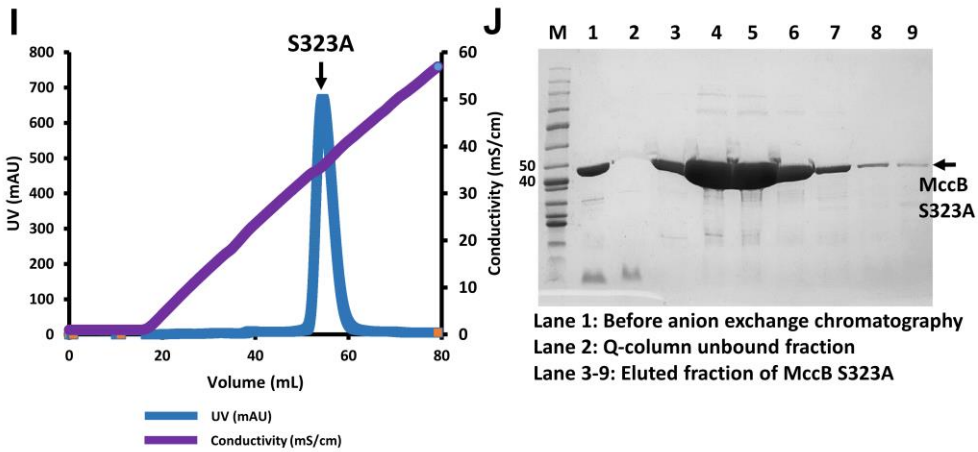

Lane 1: Before anion exchange chromatography
Lane 2: Q-column unbound fraction
Lane 3-9: Eluted fraction of MccB S323A

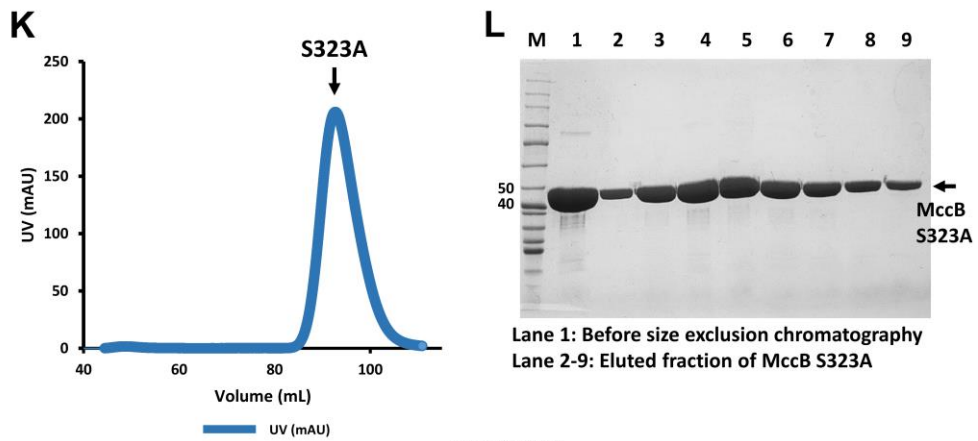

Lane 1: Before size exclusion chromatography
Lane 2-9: Eluted fraction of MccB S323A

MccB S323A

Figure 6. Purification profile of Y45F and S323A mutant MccB

A, G. SDS-PAGE analysis of Ni-NTA affinity chromatography.

B, H. SDS-PAGE analysis of His-tag cleavage using TEV protease.

C, I. UV and conductivity diagram of the Q-column elution during the anion exchange chromatography.

D, J. SDS-PAGE analysis of anion exchange chromatography

E, K. UV diagram of the superdex column elution during the size exclusion chromatography.

F, L. SDS-PAGE analysis of size exclusion chromatography.

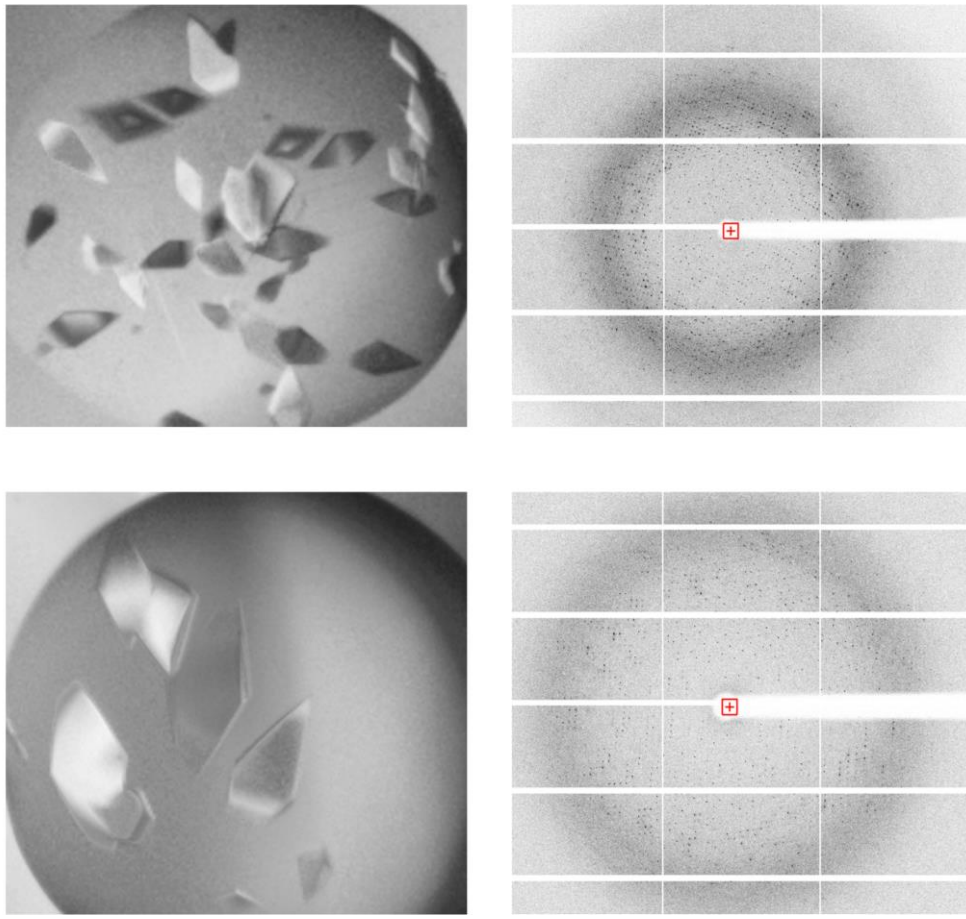

Figure 7. Crystals (left) and X-ray diffraction image (right) of Y45F mutant MccB (top) and S323A mutant MccB (bottom)

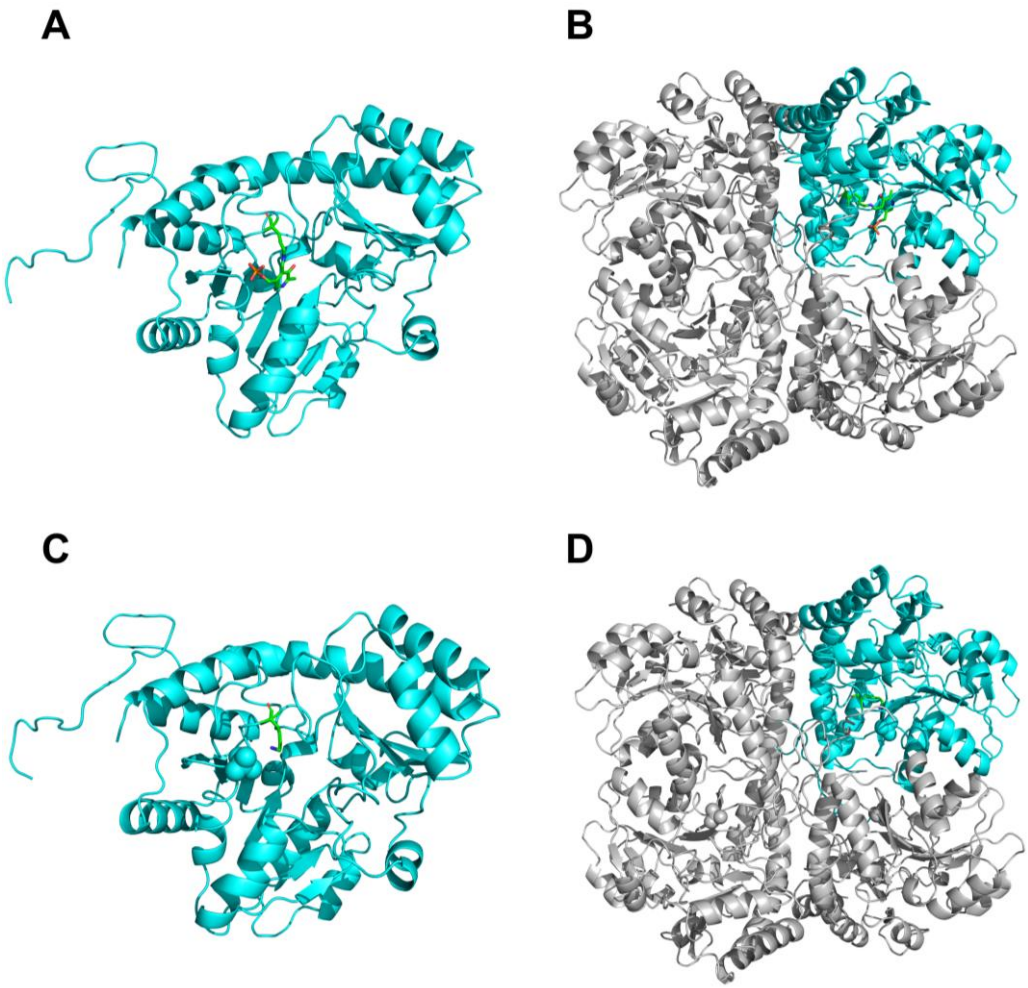

Figure 8. Overall structures of the mutant MccB in the ribbon representations

A. The asymmetric unit of Y45F mutant SaMccB consists of one protomer which is depicted by the ribbon representations in cyan.

B. The tetramer structure of Y45F mutant SaMccB. The bound PLP molecules are shown in the stick representations.

C. The asymmetric unit of S323A mutant SaMccB consists of one protomer which is depicted by the ribbon representations in cyan.

D. The tetramer structure of S323A mutant SaMccB. The Lys196 is shown in the stick representations.

3.5. The CSE and H_2S producing activities share the catalytic residues at the active site of MccB.

Both enzymatic activity assays on two mutant forms of MccB, Y45F and S323A mutants, were conducted using cystathionine or/and cysteine as substrates. As the results, both Y45F and S323A abolished the enzymatic activities, showing that all the Tyr45 and Ser323 residues are critical in the CSE from cystathionine and H_2S producing activities from cystathionine and cysteine (Fig. 9A and 9B). These findings suggested that cystathionine and cysteine are recognized by the same residues in the SaMccB active site.

Next, the crystal structures of the two mutant MccB proteins of Y45F and S323A were determined. The crystal structures of the Y45F SaMccB showed that the loop containing Phe45 became disordered, although the loop was ordered in the crystal structure of the wild-type MccB protein (Fig. 10A). The observation that the Y45F mutation abolishes the two enzyme activities of MccB, despite the presence of PLP in the active site of Y45F mutant MccB suggests that the Tyr45 plays a role in maintaining the accessibility of the substrate and the stability within the active site by opening and closing the loop from the 36 to the 48 residues. In the case of the active site of the S323A mutant MccB, the cofactor PLP disappears, which is analyzed to cause the loss of MccB activity (Fig. 10B). Considering that the Ser323 of wild-type interacts with the side chain of the Lys196 at a distance of 3.4 Å , it is analyzed that this residue plays a role in anchoring PLP at the active site of MccB.

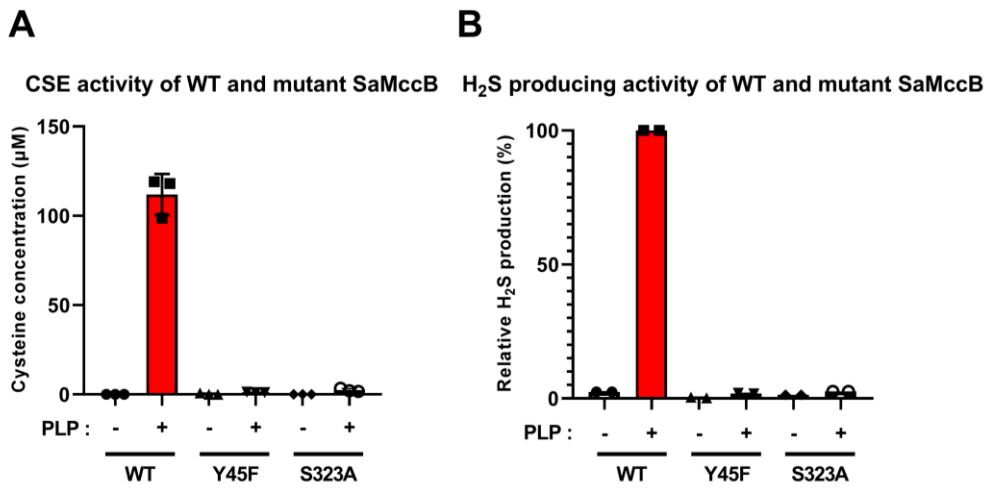

Figure 9. The cystathionine γ-lyase and the H_2S producing activities of Y45F and S323A mutant SaMccB

A. Cystathionine γ-lyase activity of the WT and mutants MccB. The reaction was initiated by injecting 200 μM cystathionine into a buffer containing 2 μM WT and mutants MccB. Absorbance of TNB was measured after 100 min reaction. The concentration of cysteine was determined based on the amount of the TNB generated. A control experiment was performed without cystathionine (n = 3, mean ± SD).

B. H_2S producing activity of the WT and mutants SaMccB. The reaction was initiated by injecting 200 μM cysteine into a buffer containing 2 μM WT and mutants MccB. Fluorescence of AMC was measured after 300 min reaction. The relative H_2S production was determined based on the fluorescence of the AMC generated. A control experiment was performed without cysteine (n = 2, mean ± SD).

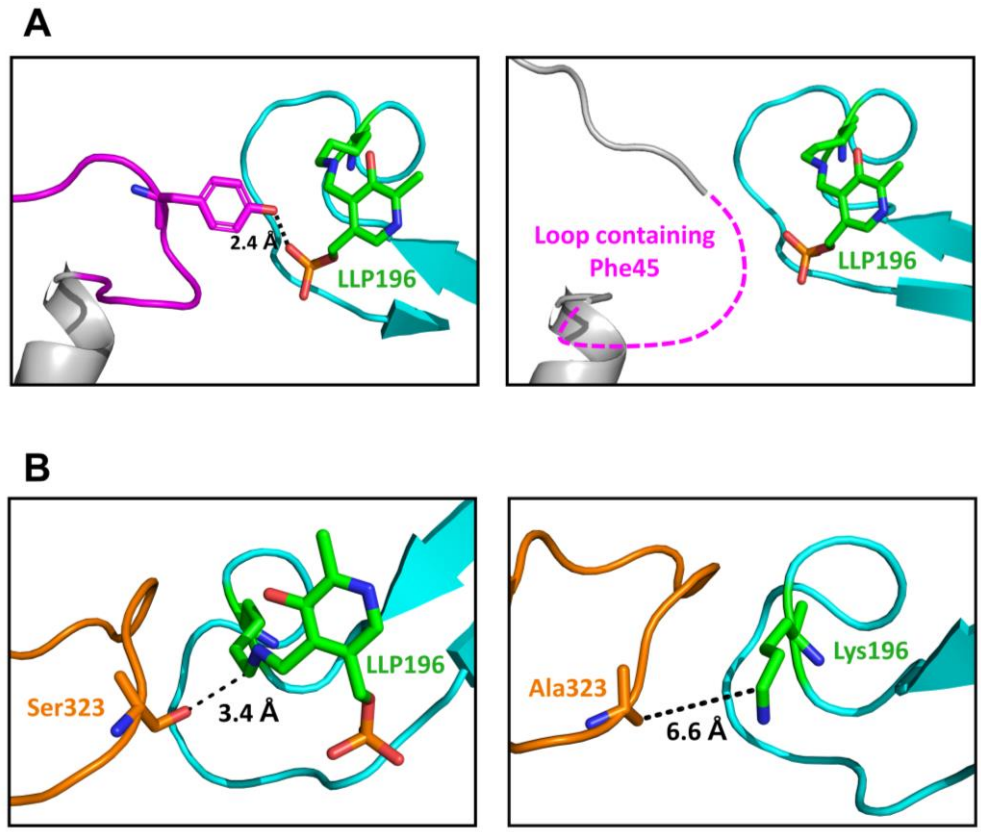

Figure 10. The structure of the active site of Y45F and S323A mutant SaMccB

A. The active site of WT (left) and Y45F SaMccB (right). Tyr45 (magenta) interacts with the phosphate group of PLP (green) at a distance of 2.4 Å in wild-type structure. The loop containing Phe45 is disappeared in the active site of Y45F mutant SaMccB.

B. The active site of WT (left) and S323A SaMccB (right). Ser323 (orange) interacts with the side chain of 196Lys (green) at a distance of 3.4 Å in wold type structure. PLP is disappeared in the active site of S323A mutant SaMccB.

3.6. SaMccB exhibited the higher activities in the PLP-supplemented buffer unlike Fn1419, not requiring the additional PLP.

The addition of PLP in the reaction was found to enhance the activities of SaMccB. The PLP were added in the reaction buffer, even though the PLP-bound form of the SaMccB protein was used, unlike CBS and MGL. To know the molecular reason why the PLP were added for the enzyme assay of SaMccB, the activities were compared with in the PLP-free reaction buffer.

In this study, the holo form of SaMccB was utilized, which was confirmed by the presence of the bound PLP (internal aldimine), as indicated by the specific absorption peak at 410 nm (Fig. 11). Interestingly, the addition of PLP to the reaction buffer significantly enhanced the H_2S-producing activities of holo MccB by approximately fourfold when cystathionine was used as the substrate (Fig. 12). This is in contrast to MGL, which did not require additional PLP in the reaction buffer for its activity (Bu, Lan et al. 2023). However, it is worth noting that the enhancement of holo MccB activity was not as pronounced when cysteine was used as the substrate in the presence of additional PLP in the buffer. These findings suggest that SaMccB exhibits a lower affinity to PLP compared to canonical PLP-dependent enzymes such as MGL. Moreover, these findings imply that SaMccB may utilize the PLP molecule differently during catalysis depending on the specific substrates employed.

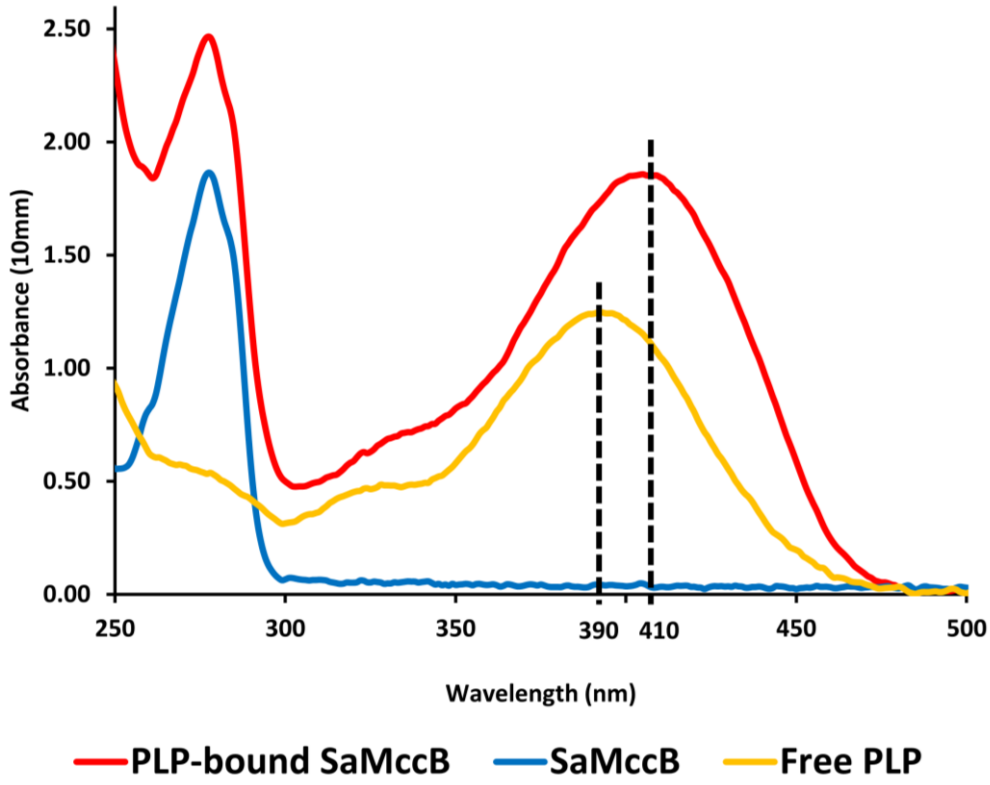

Figure 11. The absorption spectra of PLP-bound SaMccB and free-PLP

PLP and PLP-bound SaMccB exhibited absorption peaks at 390 and 410 nm, respectively.

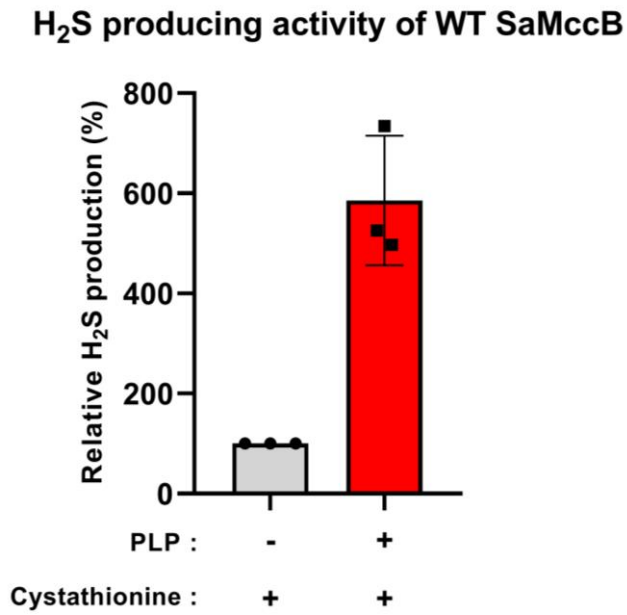

Figure 12. The H_2S producing activities of SaMccB with or without PLP

H_2S producing activity of WT SaMccB. The reaction was initiated by injecting 200 μM cystathionine into a buffer containing 2 μM WT MccB with or without 20 μM PLP. Fluorescence of AMC was measured after 300 min reaction. The relative H_2S production was determined based on the fluorescence of the AMC generated (n = 3, mean ± SD).

3.7. EGCG inhibits the H_2S producing activity of SaMccB.

I screened natural compounds for their ability to inhibit SaMccB activities on cysteine using the in-house natural compound library (Fig. 13). EGCG was found to effectively inhibit both CSE and H_2S producing activities of SaMccB at a concentration of 200uM in the reaction buffer (Fig. 14A and 14B). Moreover, EGCG exhibited dose-dependent inhibition, ranging from 2 μM to 200 μM, in subsequent experiments (Fig. 14C and 14D). EGCG reduced the H_2S producing activity of SaMccB by 90% at concentrations over 200 μM.

To see the specificity of EGCG to MccB, FN1419 was purified from Fusobacterium nucleatum (Fig. 15A-E), which is the methionine gamma-lyase that can also produce H_2S from methionine or cysteine as a canonic PLP-dependent enzyme. *Fusobacterium nucleatum*, an anaerobic oral bacterium associated with periodontal disease, produces Fn1419. EGCG exerted a more potent inhibitory effect on the H_2S producing activities of SaMccB than on Fn1419 in an H_2S assay using cysteine as the substrate (Fig. 16A and 16B), consistent with the previous results (Bu, Lan et al. 2023). Thus, these findings demonstrate that EGCG is a specific inhibitor of SaMccB.

ITC experiments were conducted to measure the dissociation constants (Kd) of SaMccB and FN1419 from Fusobacterium nucleatum. The titration curves indicated that EGCG does not bound to SaMccB (Fig. 17B), whereas FN1419 bound more strongly to EGCG with similar thermodynamic

parameters (Fig. 17A). Thus, the results demonstrated that, unlike FN1419 (Bu, Lan et al. 2023), EGCG did not form a direct complex with SaMccB. It was unusual that EGCG more strongly inhibited SaMccB despite having a weaker binding affinity compared to FN1419. I further investigated the molecular basis of this unusual observation in subsequent experiments.

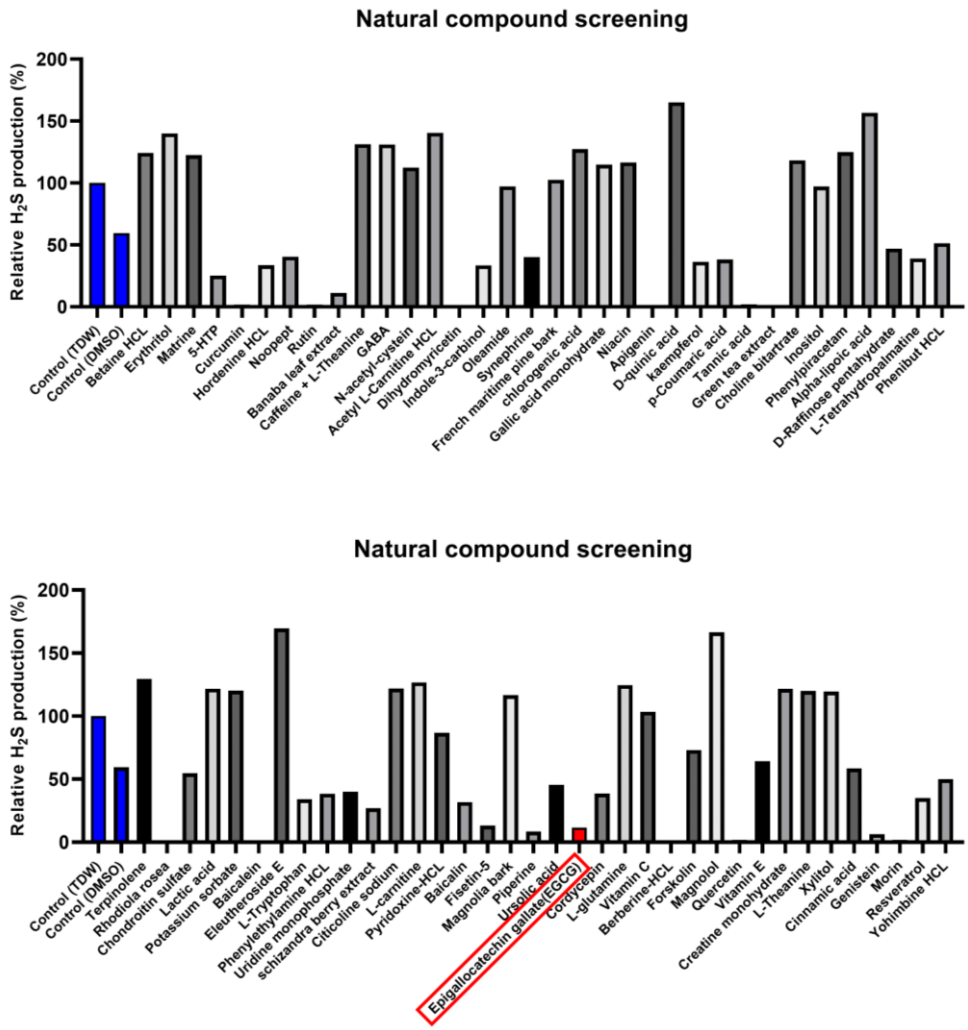

Figure 13. Screening for natural inhibitors of SaMccB

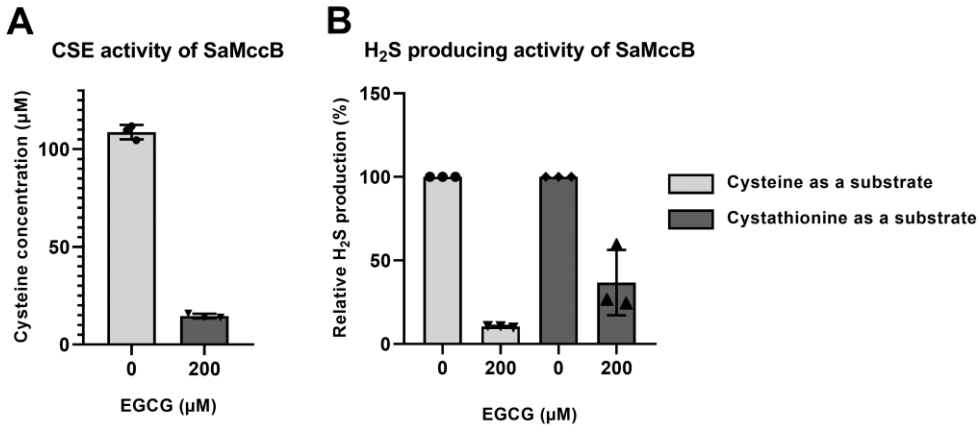
A
CSE activity of SaMccB
Cysteine concentration (μM)
100
50
0
0
200
EGCG (μM)
B
H2S producing activity of SaMccB
Relative H2S production (%)
150
100
50
0
0
200
0
200
EGCG (μM)
Cysteine as a substrate
Cystathionine as a substrate

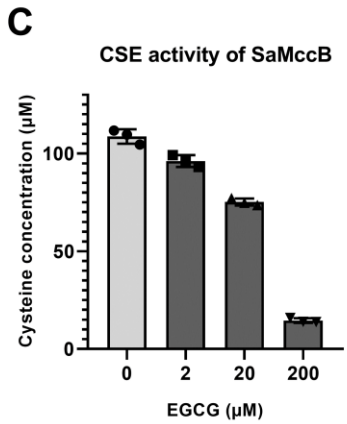
C
CSE activity of SaMccB
Cysteine concentration (μM)
100
50
0
0
2
20
200
EGCG (μM)

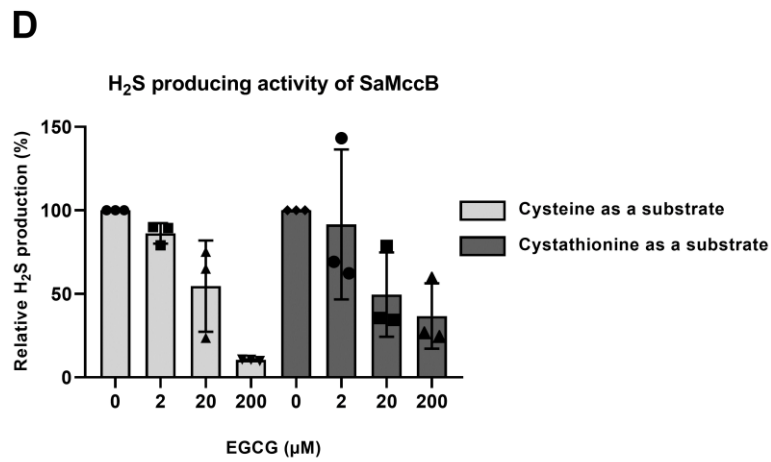
D
H2S producing activity of SaMccB
Relative H2S production (%)
150
100
50
0
0
2
20
200
0
2
20
200
EGCG (μM)
Cysteine as a substrate
Cystathionine as a substrate

Figure 14. EGCG inhibits both CSE and H_2S producing activities of SaMccB.

A. The inhibition effect of EGCG on cystathionine γ-lyase activity of MccB. The reaction was initiated by injecting 200 μM cystathionine into a buffer containing 2 μM MccB with 200 μM EGCG . Absorbance of TNB was measured after 100 min reaction. The concentration of cysteine was determined based on the amount of the TNB generated (n = 3, mean ± SD).

B. The inhibition effect of EGCG on H_2S producing activity of MccB. The reaction was initiated by injecting 200 μM cysteine or cystathionine into a buffer containing 2 μM MccB with 200 μM EGCG. Fluorescence of AMC was measured after 300 min reaction. The relative H_2S production was determined based on the fluorescence of the AMC generated (n = 3, mean ± SD).

C,D. EGCG inhibits both CSE and H_2S producing activities of SaMccB in dose-dependent manner ranging from 2 μM to 200 μM.

A

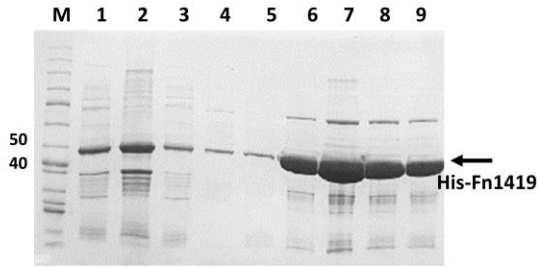

Lane 1: Supernatant fraction
Lane 2: Precipitant fraction
Lane 3: Unbound fraction
Lane 4: Washed fraction
Lane 5-9: Eluted fraction

B

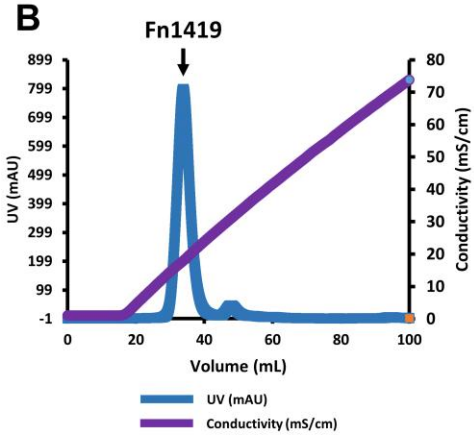

C

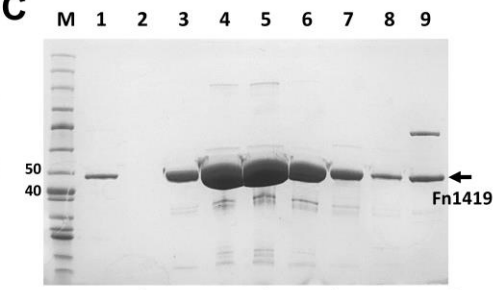

Lane 1: Before anion exchange chromatography
Lane 2: Q-column unbound fraction
Lane 3-9: Eluted fraction of Fn1419

D

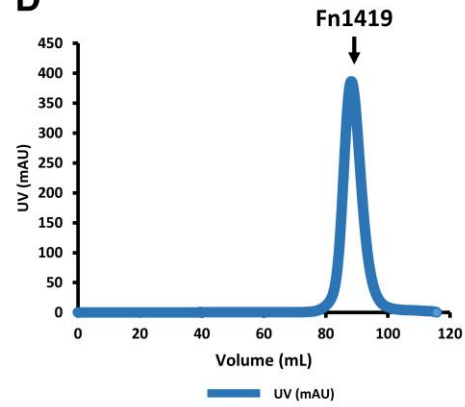

E

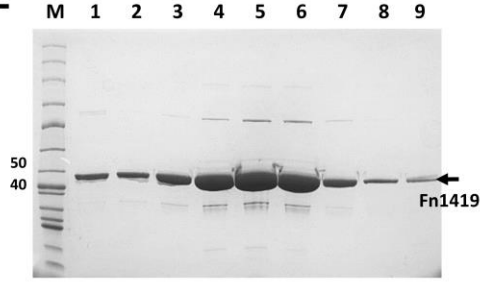

Lane 1: Before size exclusion chromatography
Lane 2-9: Eluted fraction of Fn1419

Fn1419

Figure 15. Purification profile of Fn1419

A. SDS-PAGE analysis of Ni-NTA affinity chromatography

B. UV and conductivity diagram of the Q-column elution during the anion exchange chromatography.

C. SDS-PAGE analysis of anion exchange chromatography

D. UV diagram of the superdex column elution during the size exclusion chromatography.

E. SDS-PAGE analysis of size exclusion chromatography.

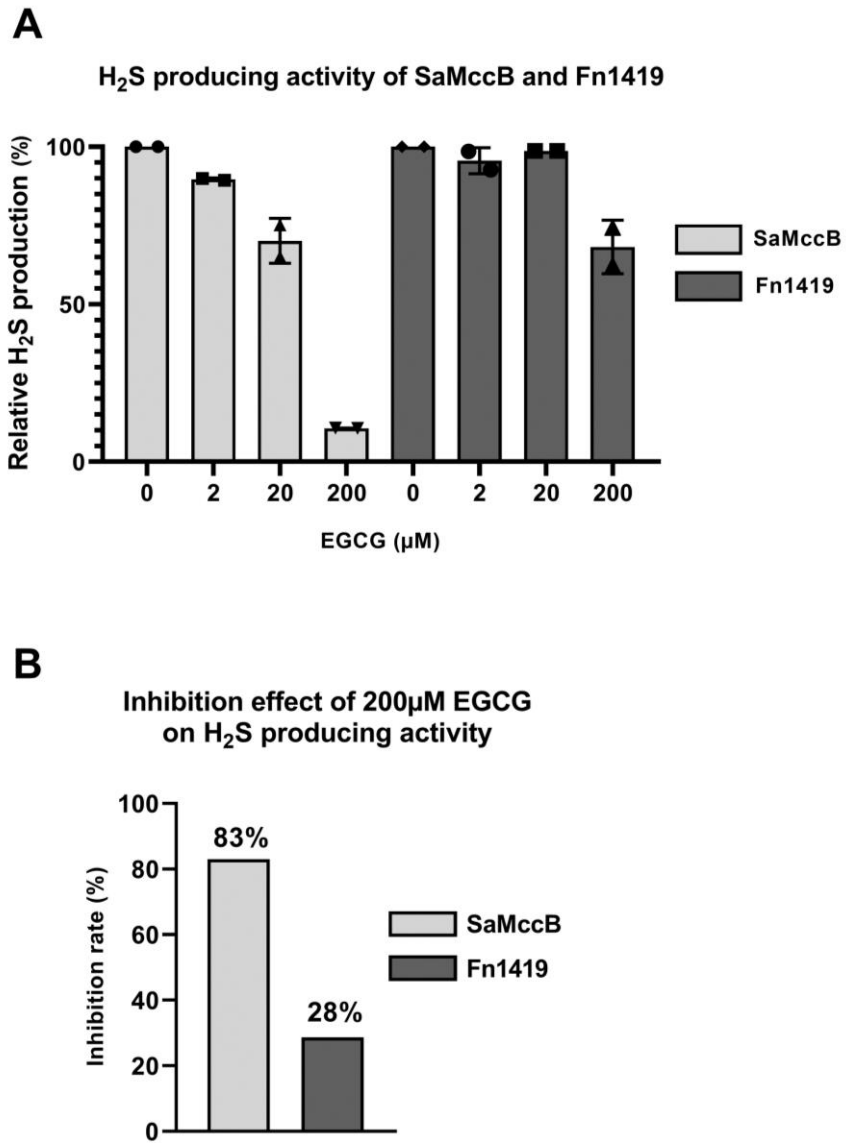

Figure 16. EGCG more strongly inhibits the H_2S producing activity of SaMccB than Fn1419.

A. The inhibition effect of EGCG ranging from 2 μM to 200 μM on H_2S producing activity of MccB and Fn1419.

B. The inhibition rate comparison of 200 μM EGCG on H_2S producing activity of MccB with Fn1419.

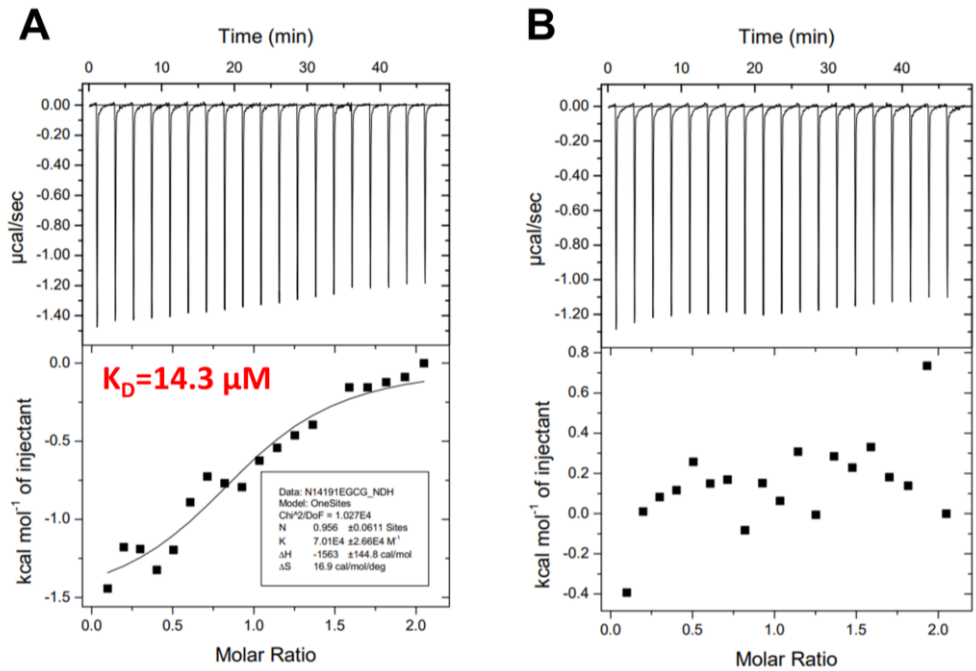

Figure 17. Isothermal titration calorimetry of the EGCG to SaMccB and Fn1419

A. ITC graph for the titration of EGCG to Fn1419. The ligand titration profile (raw data; top) and the calculated heat/enthalpy change for each titrataion (bottom) are shown in the graph. The stoichiometry value (N) and KD of Fn1419 with EGCG were calculated as one site and 14.3 µM, respectively..

B. ITC graph for the titration of EGCG to SaMccB.

3.8. EGCG make the complex with PLP in solution.

Then, how EGCG inhibited the SaMccB activity without the direct binding between them? The formation of a new complex compound between pyridoxal 5'-phosphate (PLP) and epigallocatechin gallate (EGCG) was investigated by the UV-Vis spectrophotometer. Since EGCG, the free PLP and enzyme-bound PLP in solutions have different absorption wavelengths (275nm, 390 nm, and 410 nm, respectively) (Zuhra, Petrosino et al. 2022), it was very useful to know whether the EGCG and PLP make a new complex in the buffer solution.

The UV-Vis absorption of PLP solution and purified SaMccB were analyzed to verify the binding of PLP to SaMccB. While absorption peak of free PLP in buffer solution was showed at 390 nm, the peak of binding PLP in SaMccB was showed at 410 nm (Fig. 11). Remarkably, a new absorption peak at 325 nm was found in the binary mixture of EGCG and PLP with decreased absorption peak at 275 nm from the free EGCG (Fig. 18). This observation suggested that EGCG and PLP make a putative complex, in which the electron arrangement is changed.

Next, the complex formation of epigallocatechin gallate (EGCG) and pyridoxal 5'-phosphate (PLP) was investigated using liquid chromatography-mass spectrometry (LC-MS). The LC-MS results revealed the formation of a 1:1 complex with the compound of an absorption peak at 325 nm (Fig. 19C). The molecular weight of the 325 nm-complex was determined to be 704.1026

Da, which is consistent with the sum of the molecular weights of EGCG (457.0778 Da) and PLP (246.0173 Da) (Table 2). By comparing the NMR spectra of the PLP alone, EGCG alone and the PLP-EGCG mixture, the hemi-acetal peak was detected only from the PLP-EGCG mixture (Fig. 20). Given that the aldehyde group in PLP is reactive and the EGCG contains eight hydroxyl groups, it is likely that the two molecules form an intermolecular hemiacetal compound. These findings provide insights into the mechanism of complex formation between EGCG and PLP.

In subsequent experiment, EGCG was substituted with EGC. EGC lacks the galloyl group found in EGCG but is the next most abundant catechin present in green tea (Fig. 21). EGC also produces 325 nm-complex that has the sum of the molecular weights of EGC (552.0908 Da) and PLP (246.0173 Da) when combined with PLP in a buffer solution, which is similar to EGCG (Fig. 22, Table 3). However, the quantity and diversity of peaks generated by the mixture of EGC and PLP were observed to be lower compared to the EGCG and PLP mixture. This finding indicates that EGCG has a greater yield of the new complex and suggests that EGC is less reactive to PLP than EGCG. Additionally, PLP was not fully consumed in the EGC and PLP reaction, further supporting these conclusions. The galloyl group of EGCG may play a limited role in the formation of the PLP complex.

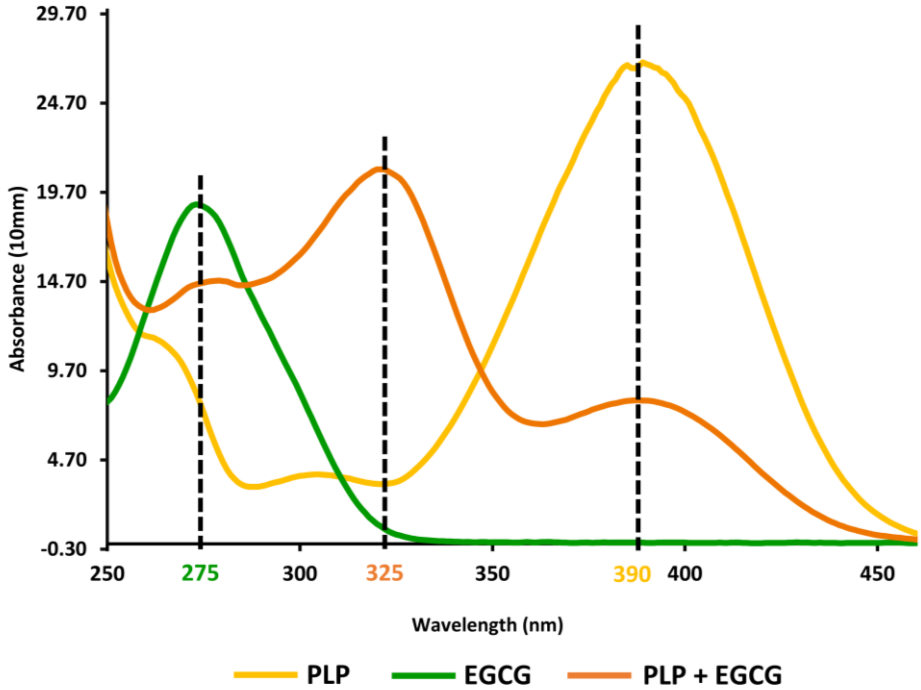

Figure 18. The absorption spectra of free-PLP, EGCG, and mixture of PLP and EGCG

Free-PLP and EGCG exhibited absorption peaks at 390 and 275 nm, respectively. The binary mixture of EGCG and PLP shows new absorption peak at 325 nm.

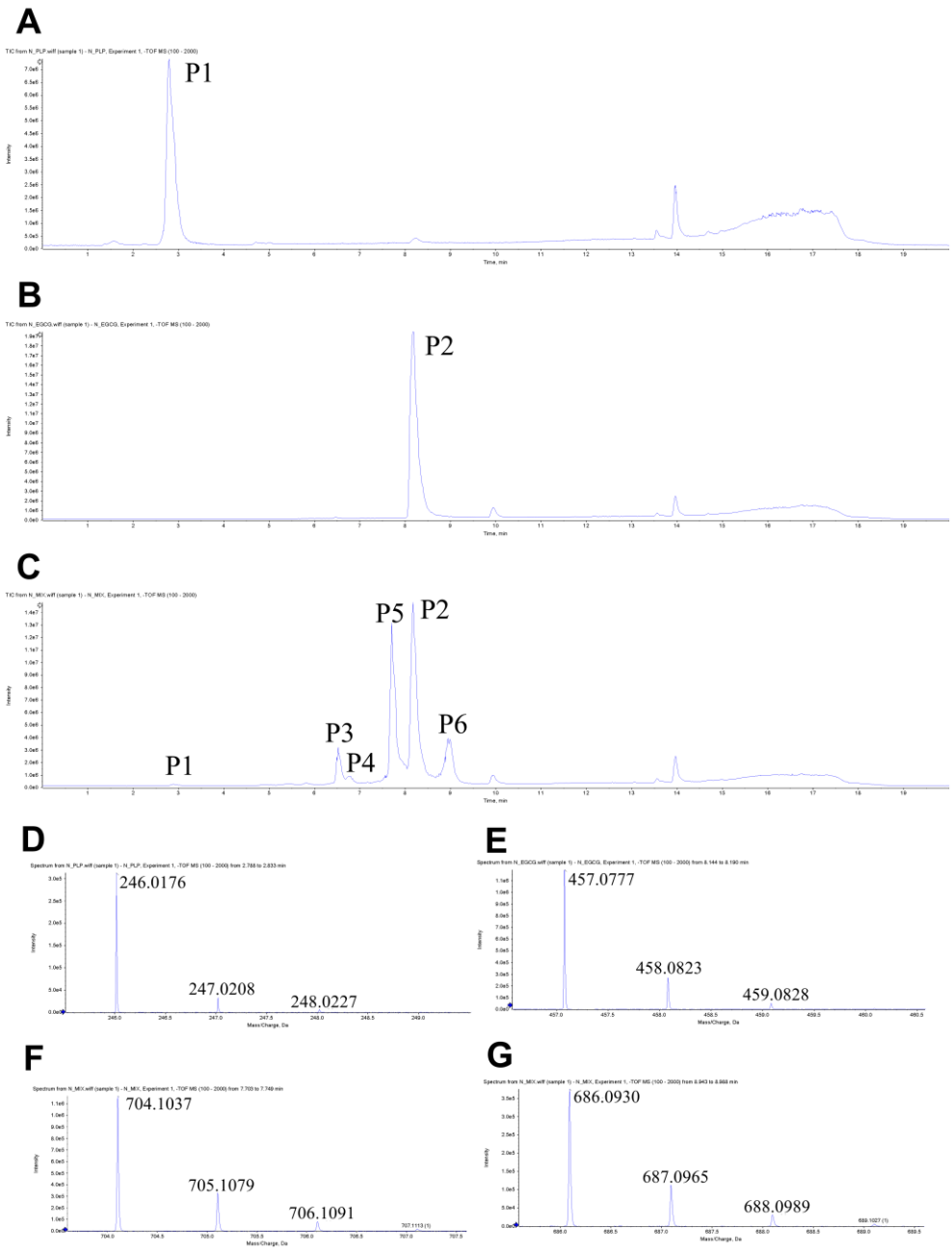
A
P1
B
P2
C
P5
P2
P3
P6
P4
P1
D
246.0176
247.0208
248.0227
E
457.0777
458.0823
459.0828
F
704.1037
705.1079
706.1091
G
686.0930
687.0965
688.0989

Figure 19. LC-MS analysis of PLP, EGCG, and mixture of PLP and EGCG

UHPLC Chromatogram of (A) PLP, (B) EGCG and (C) reacted by PLP and EGCG by UHPLC/TOF-HRMS. Peak 1, mass spectra of (D) PLP; peak 2, mass spectra of (E) EGCG; peak 3 – 5, mass spectra of (F) PLP + EGCG; peak 6, mass spectra of (G) PLP + EGCG –H2O.

Table 2. Accurate mass measurements obtained from the UHPLC/TOF-HRMS Spectra of the PLP and EGCG reaction products identified

Peak number	Compound name	Molecular Formula	Retention Time (min)	Theoretical Mass (m/z)	Measured Mass (m/z)	Mass Accuracy (ppm)
P1	PLP	C8H10NO6P	2.81	246.0173	246.0175	0.9
P2	EGCG	C22H18O11	8.17	457.0778	457.0776	0.2
P3	PLP+EGCG	C30H28NO17P	6.52	704.1022	704.1026	0.6
P4	PLP+EGCG	C30H28NO17P	6.77	704.1022	704.1029	1.0
P5	PLP+EGCG	C30H28NO17P	7.73	704.1022	704.1031	1.3
P6	PLP+EGCG – H2O	C30H26NO16P	8.96	686.0917	686.0924	1.1

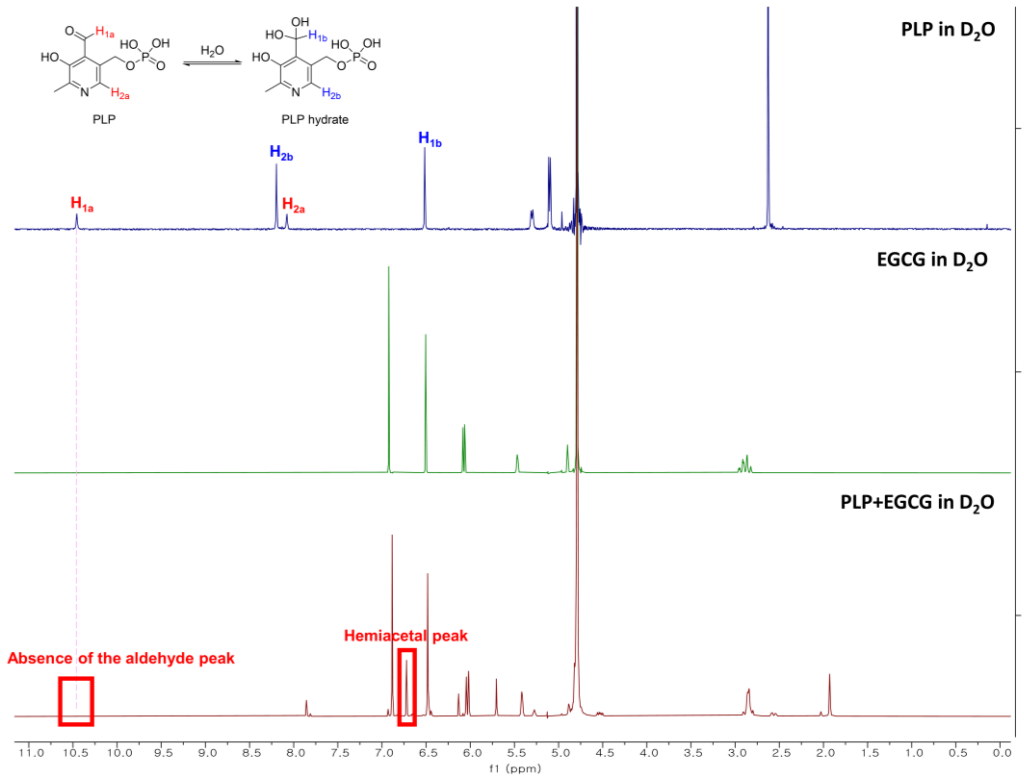

Figure 20. NMR analysis of PLP and EGCG complex

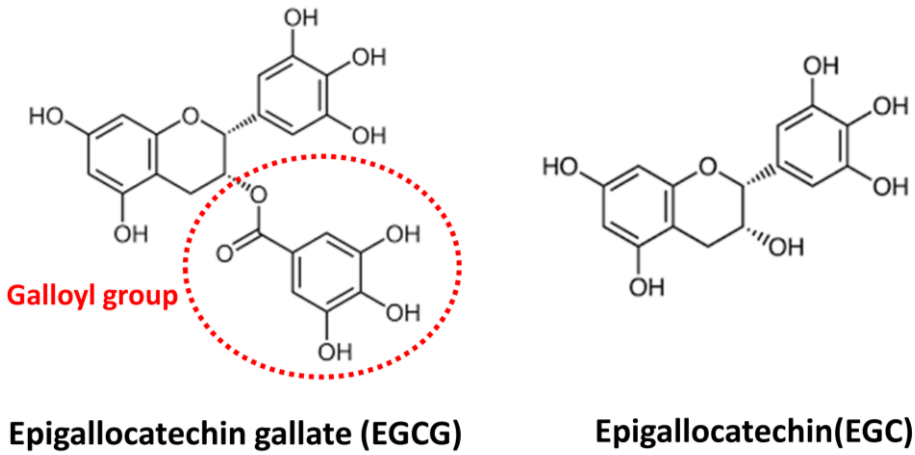

Figure 21. Chemical structures of EGCG and EGC

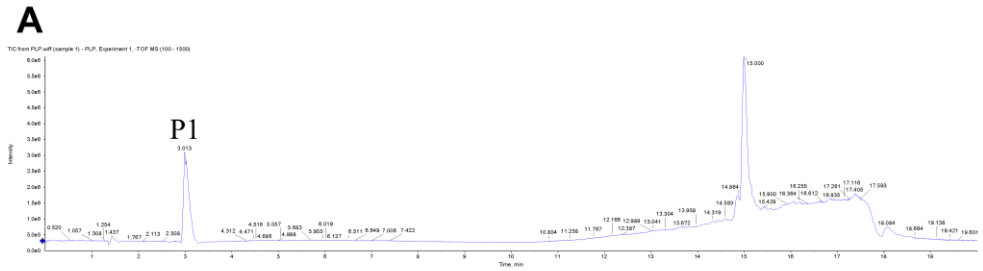
A
P1
3.013
Intensity
Time, min

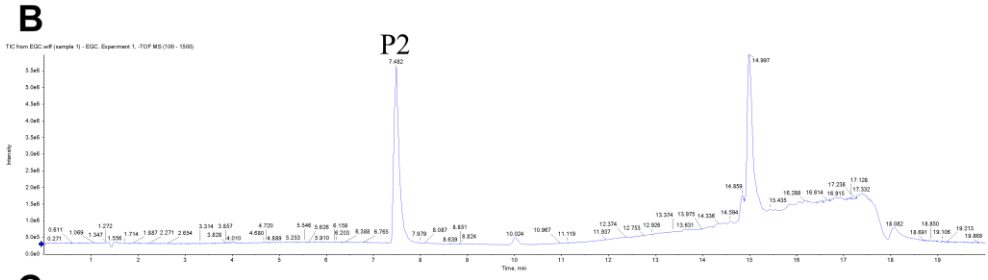
B
P2
7.482
14.997
Intensity
Time, min

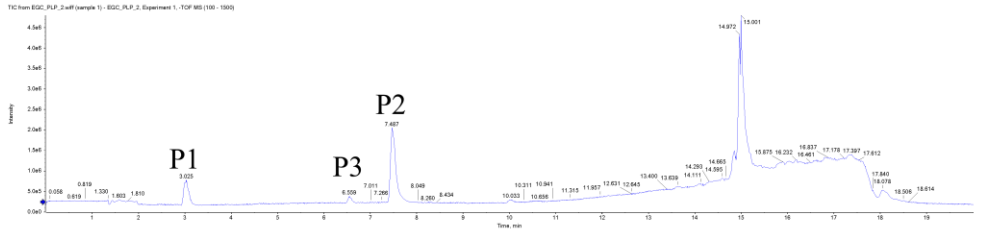
C
P1
3.023
P2
7.487
P3
14.972
15.001
Intensity
Time, min

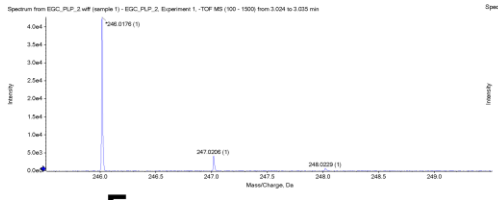
D
Spectrum from EGC_PLP_2.wiff (sample 1) - EGC_PLP_2, Experiment 1, -TOF MS (100 - 1500) from 3.024 to 3.035 min
*246.0176 (1)
247.0206 (1)
248.0239 (1)
Intensity
Mass/Charge, Da

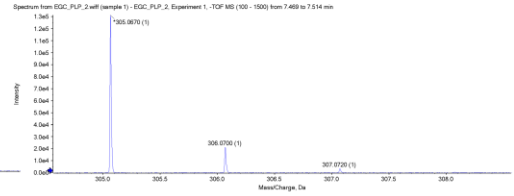
E
Spectrum from EGC_PLP_2.wiff (sample 1) - EGC_PLP_2, Experiment 1, -TOF MS (100 - 1500) from 7.469 to 7.514 min
*305.0670 (1)
306.0700 (1)
307.0720 (1)
Intensity
Mass/Charge, Da

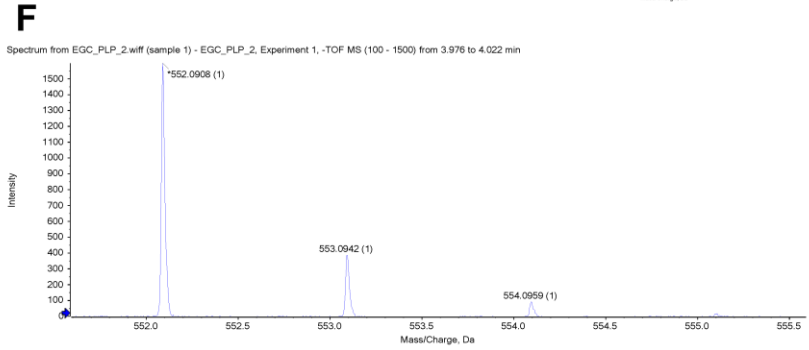
F
Spectrum from EGC_PLP_2.wiff (sample 1) - EGC_PLP_2, Experiment 1, -TOF MS (100 - 1500) from 3.976 to 4.022 min
*552.0908 (1)
553.0942 (1)
554.0959 (1)
Intensity
Mass/Charge, Da

Figure 22. LC-MS analysis of PLP, EGC, and mixture of PLP and EGC

UHPLC Chromatogram of (A) PLP, (B) EGC and (C) reacted by PLP and EGCG by UHPLC/TOF-HRMS. Peak 1, mass spectra of (D) PLP; peak 2, mass spectra of (E) EGC; peak 3, mass spectra of (F) PLP + EGCG.

Table 3. Accurate mass measurements obtained from the UHPLC/TOF-HRMS Spectra of the PLP and EGC reaction products identified

Peak number	Compound name	Molecular Formula	Retention Time (min)	Theoretical Mass (m/z)	Measured Mass (m/z)	Mass Accuracy (ppm)
P1	PLP	C8H10NO6P	3.03	246.0173	246.0175	0.9
P2	EGC	C15H14O7	7.48	305.0669	305.0678	2.3
P3	PLP+EGC	C23H24NO13P	4.01	552.0913	552.0908	-0.8

3.9. EGCG inhibits SaMccB by abstracting PLP from the enzyme active site.

Considering the complex formation of EGCG and PLP in solution, the ability of EGCG to abstract the bound PLP at the active site of MccB was investigated. The PLP-bound MccB protein was first prepared by removing all free PLP from the PLP-containing MccB protein sample. Then, the dialyzed protein samples were treated with 200 μM EGCG and a UV-Vis spectrophotometer was used to detect the formation of the previously observed new complex peak at 325 nm. Surprisingly, a new absorption peak at 325 nm was detected, indicating that EGCG abstracted the PLP molecule from the MccB protein (Fig. 23A). Consistently, the addition of 200 μM EGCG to the PLP-bound MccB protein sample decreased the absorption peak at 410 nm, indicating the MccB-bound PLP molecule (Fig. 24A).

In the same experiment with the PLP-bound Fn1419 protein, EGCG was unable to abstract the PLP molecule from Fn1419 (Fig. 24B). These results demonstrated that EGCG could not abstract the strongly-bound PLP molecule at the enzyme's active site. These findings suggest that EGCG can abstract only the loosely-bound PLP at the active site of MccB but not the strongly-bound PLP. This indicates that the inhibitory mechanism of EGCG on PLP-dependent enzymes SaMccB and Fn1419 does not involve direct binding between EGCG and the enzymes, but rather is responsible for the abstraction of PLP from the enzyme's active site.

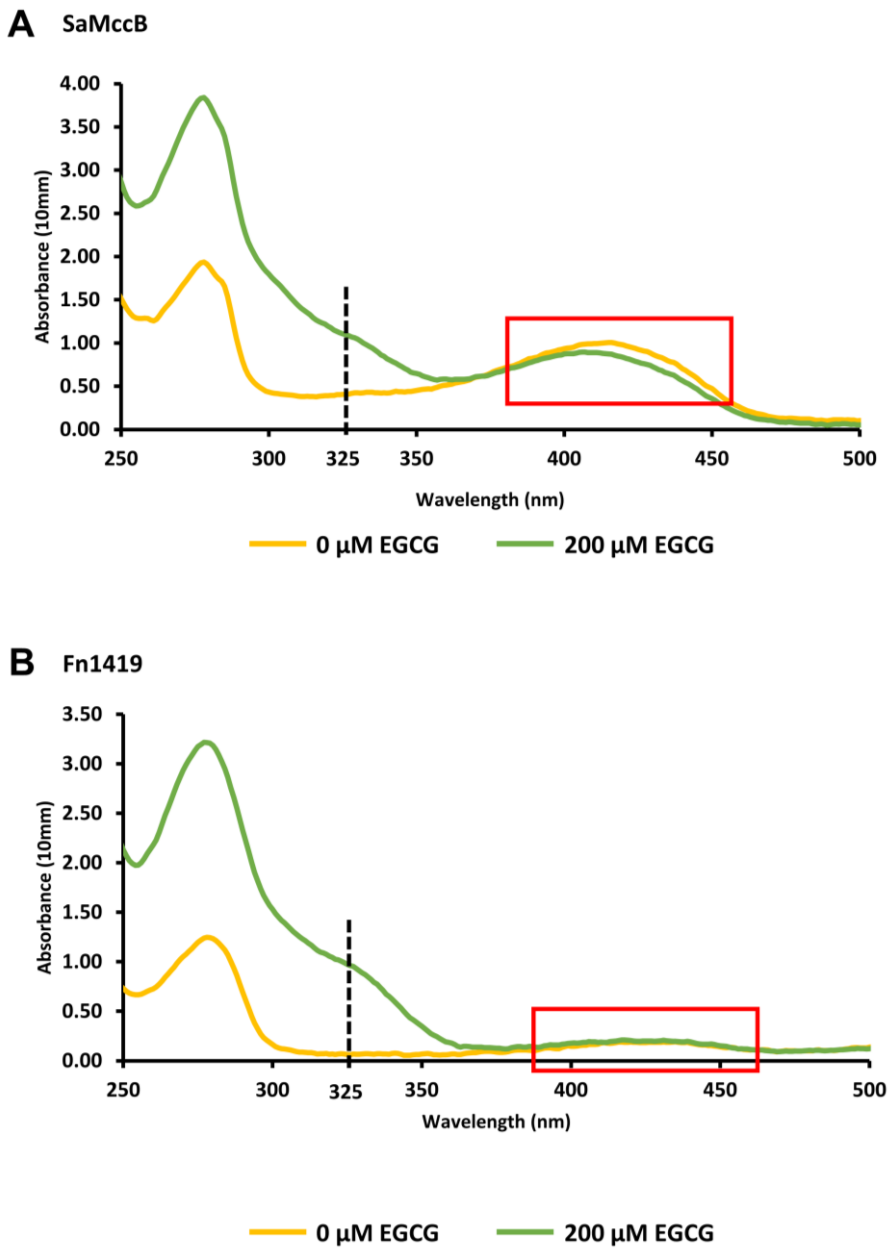

Figure 23. The absorption spectra of SaMccB and Fn1419 with or without EGCG

A. The absorption spectra of SaMccB with (green) or without (yellow) 200 μM EGCG.

B. The absorption spectra of Fn1419 with (green) or without (yellow) 200 μM EGCG.

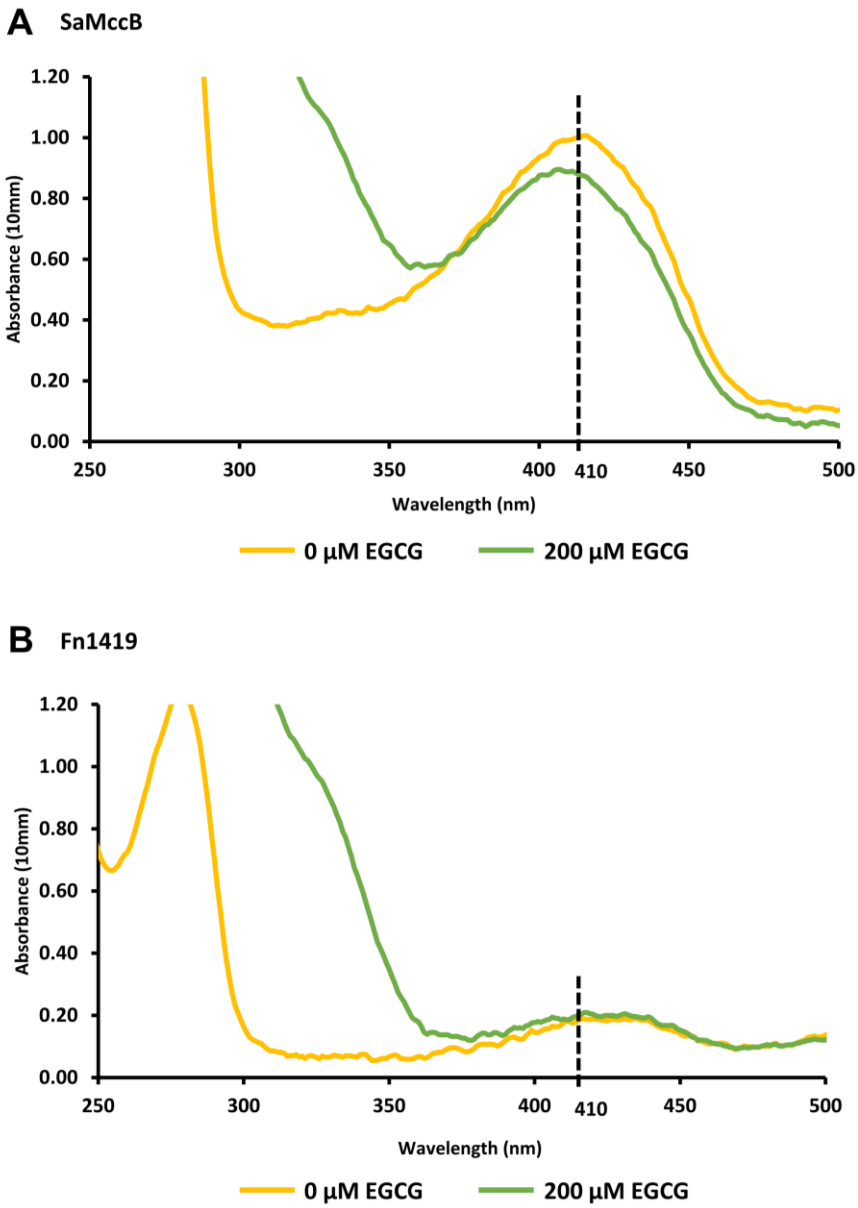

Figure 24. The absorption spectra of bound-PLP of SaMccB and Fn1419 with or without EGCG

A. The absorption spectra of bound-PLP of SaMccB with (green) or without (yellow) 200 µM EGCG. The box from Figure 23 is enlarged. The absorption peak of 410 nm decreased after the treatment of EGCG.

B. The absorption spectra of bound-PLP of Fn1419 with (green) or without (yellow) 200 μM EGCG. The box from Figure 23 is enlarged. The absorption peak of 410 nm did not decrease after the treatment of EGCG.

3.10. Treatment of EGCG reduced the H_2S production in the SaMccB-overproducing bacteria

200 μM of EGCG can reduce the H_2S production of PLP-dependent enzymes. Next, whether EGCG has potential to inhibit hydrogen sulfide production in SaMccB-expressing *E. coli* was also investigated. SaMccB was strongly induced in the *E. coli* cell cultured in the M9 medium by the addition of IPTG. Upon induction of SaMccB in the bacteria, the H_2S production was significantly increased, demonstrating that the H_2S production by the bacteria is the results of the SaMccB activity (Fig. 25A). Treatment of 200 μM and 2 mM EGCG to the *E. coli* cells abolished the H_2S production. EGCG showed a inhibitory effect on the bacteria in the H_2S production at the same concentration to the biochemical assay, EGCG would have a reasonable permeability to the bacterial cell membrane.

When the bacterial cells were disrupted by sonication, EGCG strongly inhibited the H_2S production activity in the cell lysate at 200 μM (Fig. 25B). Thus, it can be suggested that the increasing permeability of EGCG to the cytosol of the bacterial cells can enhance the inhibitory effect on H_2S producing activity of the bacteria.

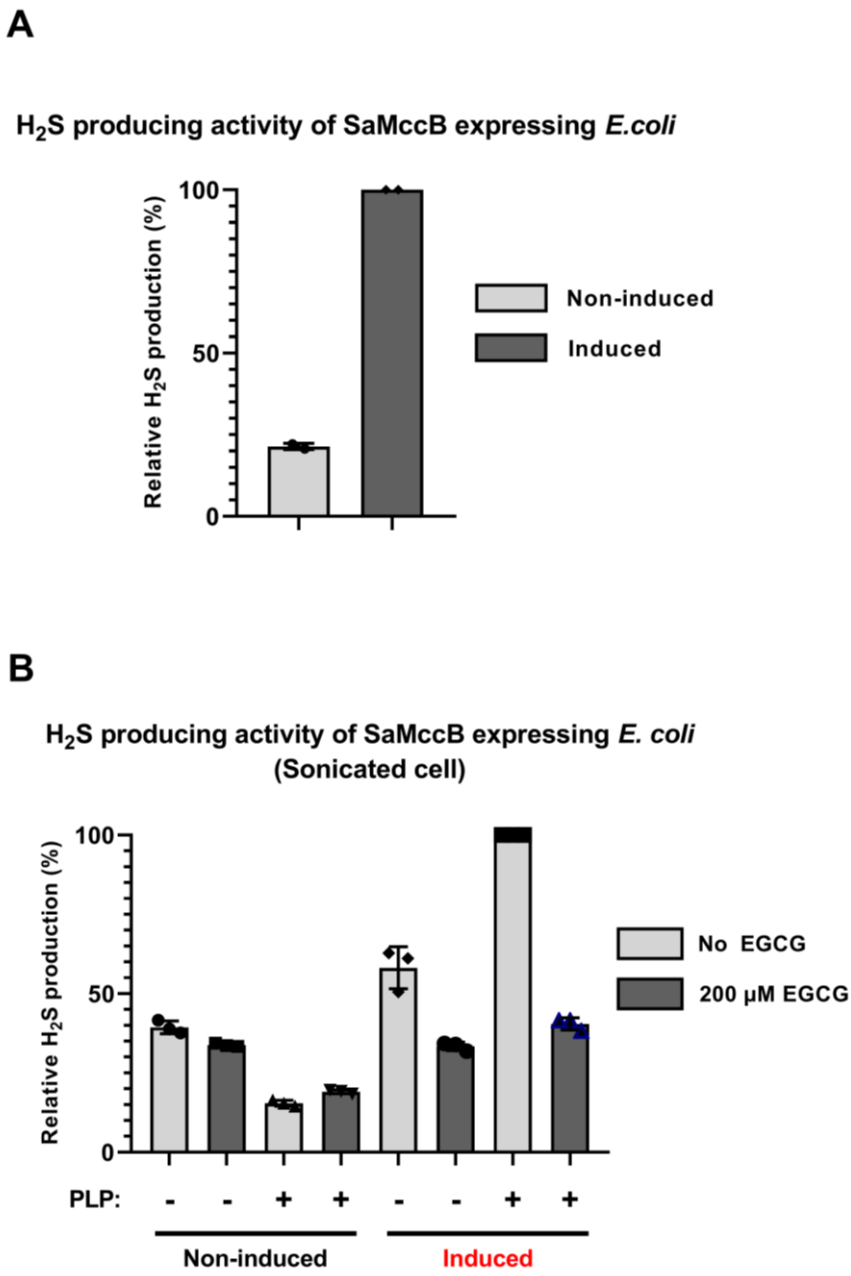

Figure 25. The H_2S producing activities of SaMccB expressing *E. coli*

A. H_2S producing activity of SaMccB expressing *E. coli.* The reaction was initiated by injecting 200 μM cysteine into a buffer containing induced or non-induced SaMccB expressing *E. coli* cell respectively. Fluorescence of

AMC was measured after 300 min reaction. The relative H_2S production was determined based on the fluorescence of the AMC generated (n = 2, mean ± SD).

B. The inhibition effect of EGCG on H_2S producing activity of SaMccB expressing *E. coli* disrupted by sonication.

3.11. EGCG could reduce the H_2S production in the *S. aureus* whereas, it could not inhibit the H_2S production by the probiotics *Lactobacillus*.

200 μM of EGCG could reduce the H_2S production from SaMccB-overproducing *E.coli*. Next, whether EGCG also inhibit hydrogen sulfide production in *Staphylococcus aureus* and the probiotics *Lactobacillus plantarum* was investigated. The results indicate that epigallocatechin gallate at a concentration of 200 μM inhibits hydrogen sulfide production in *Staphylococcus aureus* (Fig. 26). Interestingly, it does not have the same effect on beneficial gut microbiota such as *Lactobacillus plantarum* (Fig. 26). These findings propose that the inhibitory mechanism of EGCG on hydrogen sulfide synthesis is potentially strain-specific, particularly towards *Staphylococcus aureus*.

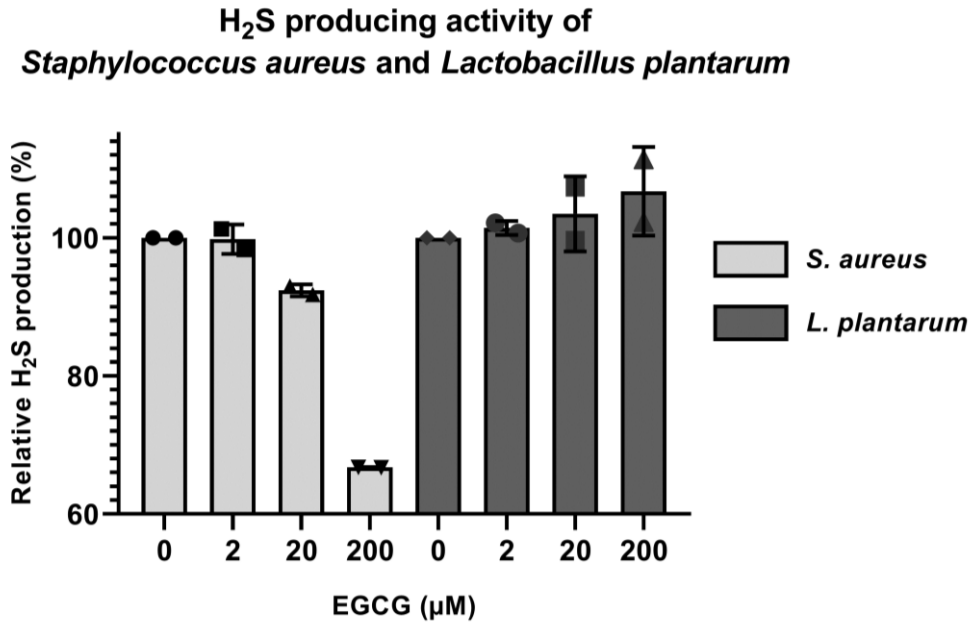

Figure 26. The H_2S producing activities of *S. aureus* and *L. plantarum*

The inhibition effect of EGCG ranging from 2 μM to 200 μM on H_2S producing activity of *S. aureus* and *L. plantarum*. The reaction was initiated by injecting 200 μM cysteine into a buffer *S. aureus* or *L. plantarum* cell respectively. Fluorescence of AMC was measured after 300 min reaction. The relative H_2S production was determined based on the fluorescence of the AMC generated (n = 2, mean ± SD).

IV. Discussions

In this study, the CSE and H_2S producing activities of MccB were investigated, which is known as the primary H_2S producer in *S. aureus*. Structure-based mutational studies revealed that the residues lining the substrate binding site are commonly utilized by both CSE and H_2S producing activities of MccB, indicating shared substrate binding mechanisms. The major green tea catechin, EGCG, was identified as a potent inhibitor of SaMccB's H_2S production. Interestingly, EGCG inhibited MccB through a non-canonical mechanism that was neither competitive nor non-competitive. EGCG formed a complex with free PLP in solution, which further extracted the bound PLP at the active site. However, EGCG failed to inhibit H_2S production by Fn1419 and was unable to extract the strongly-bound PLP from the Fn1419 active site. Experiments with MccB-overexpressing *E. coli* and *S. aureus* showed consistent results with EGCG; treatment with EGCG significantly decreased H_2S production levels in bacterial cells. These findings suggest that the direct binding of EGCG to the enzyme is not essential for inhibiting its enzymatic activities. Instead, PLP abstraction occurs via a chemical equilibrium between bound and free PLP. The mass and UV spectrophotometric results indicate that EGCG forms a covalent complex with PLP, possibly through hemiacetal formation. Although this hemiacetal compound is not stable in solution, EGCG can shift the equilibrium towards the abstraction of bound PLP into the solution by forming a hemiacetal

complex with PLP.

EGCG has been noted as an anti-inflammatory compound. Thus, it is noteworthy a mechanism through the inhibition of the H_2S production in gut since H_2S promotes inflammation in humans (Zhang, Li et al. 2021). EGCG is the primary catechin in green tea, accounting for 50% to 80% and representing 200 to 300 mg per brewed cup of green tea, or 2-3 mg/mL (Qin, Xie et al. 2007). In addition to its inhibitory effects on H_2S production, EGCG has demonstrated other beneficial effects in studies related to diabetes, Parkinson's disease, Alzheimer's disease, stroke, and obesity, and possesses antioxidant properties (Chacko, Thambi et al. 2010). Also, EGCG has been studied that it has effect on reducing the anti-resistance of S. aureus (Zhao, Hu et al. 2001). While achievable concentrations of 2 mM EGCG (~1 mg/mL, MW 458 Da) are only possible if EGCG is localized, green tea still provides sufficient concentration and amount to reduce the levels of free PLP or pyridoxal in the gastrointestinal tract, thereby inhibiting H_2S production by inhibiting MccB or its homologues in bacteria. This uptake of green tea may contribute to reducing the tolerance of *S. aureus* to treated antibiotics in the gut since H_2S in the gut has been associated with increased antibiotic resistance of *S. aureus*. It is also noteworthy that excess doses of PLP can cause various side effects, including skin rashes and nerve damage (Vrolijk, Opperhuizen et al. 2017). EGCG in green tea may help remove the excess PLP by forming a hemiacetal complex.

It has been observed that EGCG at a concentration of 200μM inhibits the production of hydrogen sulfide in *Staphylococcus aureus*, but it does not inhibit the production of hydrogen sulfide in *Lactobacillus plantarum*, which known as beneficial bacterium found in the gut. This suggests that the hydrogen sulfide inhibitory effects of EGCG may be specific to *Staphylococcus aureus*.

In conclusion, the study discovered a new mode of action of EGCG in inhibition of the PLP-dependent enzyme using biochemical and cellular assays.

V. References

Adams, P. D., et al. (2010). "PHENIX: a comprehensive Python-based system for macromolecular structure solution." Acta crystallographica section D: biological crystallography 66(2): 213-221.

Bu, T., et al. (2023). "Structural Basis of the Inhibition of L-Methionine γ-Lyase from Fusobacterium nucleatum." International Journal of Molecular Sciences 24(2): 1651.

Chacko, S. M., et al. (2010). "Beneficial effects of green tea: a literature review." Chinese medicine 5(1): 1-9.

Druzhyna, N., et al. (2016). "Screening of a composite library of clinically used drugs and well-characterized pharmacological compounds for cystathionine β-synthase inhibition identifies benserazide as a drug potentially suitable for repurposing for the experimental therapy of colon cancer." Pharmacological research 113: 18-37.

Edelheit, O., et al. (2009). "Simple and efficient site-directed mutagenesis using two single-primer reactions in parallel to generate mutants for protein structure-function studies." BMC biotechnology 9(1): 1-8.

Joshi, P., et al. (2019). "Insights into multifaceted activities of CysK for therapeutic interventions." 3 Biotech 9: 1-16.

Lee, D., et al. (2019). "Crystal structure of bacterial cystathionine γ-lyase in the cysteine biosynthesis pathway of Staphylococcus aureus." Crystals 9(12): 656.

Otwinowski, Z. and W. Minor (1997). [20] Processing of X-ray diffraction data collected in oscillation mode. Methods in enzymology, Elsevier. 276: 307-326.

Percudani, R. and A. Peracchi (2003). "A genomic overview of pyridoxal-phosphate-dependent enzymes." EMBO reports 4(9): 850-854.

Qin, J., et al. (2007). "A component of green tea,(−)-epigallocatechin-3-gallate, promotes apoptosis in T24 human bladder cancer cells via modulation of the PI3K/Akt pathway and Bcl-2 family proteins." Biochemical and biophysical research communications 354(4): 852-857.

Shatalin, K., et al. (2021). "Inhibitors of bacterial H_2S biogenesis targeting

antibiotic resistance and tolerance." Science 372(6547): 1169-1175.

Shatalin, K., et al. (2011). "H_2S: a universal defense against antibiotics in bacteria." Science 334(6058): 986-990.

Singh, S. and R. Banerjee (2011). "PLP-dependent H_2S biogenesis." Biochimica et Biophysica Acta (BBA)-Proteins and Proteomics 1814(11): 1518-1527.

Thorson, M. K., et al. (2013). "Identification of cystathionine β-synthase inhibitors using a hydrogen sulfide selective probe." Angewandte Chemie International Edition 52(17): 4641-4644.

Vrolijk, M. F., et al. (2017). "The vitamin B6 paradox: Supplementation with high concentrations of pyridoxine leads to decreased vitamin B6 function." Toxicology in Vitro 44: 206-212.

Zhang, C., et al. (2021). "Epigallocatechin-3-gallate prevents inflammation and diabetes-Induced glucose tolerance through inhibition of NLRP3 inflammasome activation." International Immunopharmacology 93: 107412.

Zhao, W.-H., et al. (2001). "Mechanism of synergy between epigallocatechin gallate and β-lactams against methicillin-resistant Staphylococcus aureus." Antimicrobial agents and chemotherapy 45(6): 1737-1742.

Zuhra, K., et al. (2022). "Epigallocatechin gallate is a potent inhibitor of cystathionine beta-synthase: Structure-activity relationship and mechanism of action." Nitric Oxide 128: 12-24.

VI. 국문초록

황색포도상구균은 피리독살 인산-의존성 효소인 MccB를 통하여 황화수소를 생성하며 이는 병원균의 지속적인 생존력과 항생제 저항성을 증가시키는 것으로 알려져 있다. 본 연구에서는 황색포도상구균 MccB의 결정 구조 규명을 통하여 피리독살 인산이 존재하는 활성부위 주변에 반응에 관여하는 잔기들을 확인하였다. 이 잔기들의 돌연변이화에 의하여 MccB의 효소 활동이 없어짐을 확인하였으며 돌연변이 MccB 결정 구조가 MccB의 시스타티온 감마 라이에이즈 활성과 황화수소 생성 활성이 공통적으로 MccB의 활성 부위에 있는 잔기들에 의하여 촉매된다는 것을 보여주었다.

또한, MccB의 두가지 활성을 조사하고, MccB 단백질의 활성에 대한 천연물의 억제 효과를 탐색하였다. 정제된 황색포도상구균 MccB는 시스타티온에서 시스테인을 생산하는 시스타티온 감마 라이에이즈 활성과 시스테인으로부터 황화수소를 생성하는 활성을 나타내었다. 또한 천연물 스크리닝을 통하여 차 카테킨의 주 성분인 에피갈로카테킨 갈레이트가 MccB 단백질의 활성을 강력하게 억제함을 발견하였다. 에피갈로카테킨 갈레이트는 MccB의 보조인자인 피리독살 인산과 결합하여 헤미아세탈 구조를 이룸으로써 MccB를 억제하며, 이로 인해 세포질 내 자유 피리독살 인산 양이

줄어든다.

에피갈로카테킨 갈레이트는 또한 MccB 과발현 세균과 황색포도상구균에서 황화수소를 감소시켰다. 흥미롭게도, 락토바실러스 플란타럼에서의 황화수소 생산은 억제하지 못하였는데, 이는 에피갈로카테킨 갈레이트의 황화수소 생산에 대한 억제 효과가 특정 균주, 특히 황색포도상구균에 특정됨을 알 수 있다. 본 연구는 에피갈로카테킨 갈레이트가 세균의 황화수소 생산을 조절하는 새로운 경로에 대한 이해를 제공하며, 각종 차로 섭취 가능한 에피갈로카테킨 갈레이트가 황화수소로 인해 야기되는 장 내 염증과 대장암 발병을 억제함과 동시에 병원균의 항생제 내성을 줄일 수 있음을 시사한다.

주요어: 황화수소, 황색포도상구균, 항생제 내성, MccB, 피리독살 인산, 에피갈로카테킨 갈레이트, 시스타티온 감마 라이에이즈 활성, 황화수소 생성 활성

학번: 2021-24928